© 2024. Published by The Company of Biologists Ltd | Development (2024) 151, dev202694. doi:10.1242/dev.202694

RESEARCH ARTICLE

A role for BYN-1/bystin in cellular uptake and clearance of residual bodies in the *Caenorhabditis elegans* germline

Hyemin Min*, Emily L. Spaulding, Catherine S. Sharp, Pankaj Garg, Esther Jeon, Lyn S. Miranda Portillo, Noah A. Lind and Dustin L. Updike‡

ABSTRACT

GLH/Vasa/DDX4 helicases are core germ-granule proteins that promote germline development and fertility. A yeast-two-hybrid screen using *Caenorhabditis elegans* GLH-1 as bait identified BYN-1, the homolog of human bystin/BYSL. In humans, bystin promotes cell adhesion and invasion in gliomas, and, with its binding partner trophinin, triggers embryonic implantation into the uterine wall. *C. elegans* embryos do not implant and lack a homolog of trophinin, but both trophinin and GLH-1 contain unique decapeptide phenylalanine-glycine (FG)-repeat domains. In germ cells, we find endogenous BYN-1 in the nucleolus, partitioned away from cytoplasmic germ granules. However, BYN-1 enters the cytoplasm during spermatogenesis to colocalize with GLH-1. Both proteins become deposited in residual bodies (RBs), which are then engulfed and cleared by the somatic gonad. We show that BYN-1 acts upstream of CED-1 to drive RB engulfment, and that removal of the FG-repeat domains from GLH-1 and GLH-2 can partially phenocopy *byn-1* defects in RB clearance. These results point to an evolutionarily conserved pathway whereby cellular uptake is triggered by the cytoplasmic mobilization of bystin/BYN-1 to interact with proteins harboring FG-repeats.

KEY WORDS: Bystin, BYN-1, GLH-1, Trophinin, FG-repeat, Residual bodies

INTRODUCTION

GLH/Vasa/DDX4 plays a crucial role in germline development of metazoans, yet it is just one of several DEAD-box RNA helicases present in an animal's genome. Setting Vasa apart from other DEAD-box proteins are three additional domains surrounding its structured helicase: a glycine-rich repeat motif, a flanking domain wrapping around the helicase, and a negatively charged domain preceding a terminal tryptophan (Sengoku et al., 2006). In *Drosophila*, Vasa's helicase domain interacts with Piwi Argonaute proteins in a transient piRNA amplifier complex (Xiol et al., 2014). Similarly, in *Caenorhabditis elegans*, the Argonaute proteins CSR-1 and PRG-1 have been identified in GLH immunoprecipitation and proximity labeling studies, indicating that they likely form a complex analogous to *Drosophila*'s transient piRNA amplifier complex (Chen et al., 2020; Marnik et al., 2019; Price et al., 2021). However, little is known about germline proteins that interface with the Vasa-defining peripheral domains.

In *C. elegans*, the paralogs GLH-1 and GLH-2 are the only DEAD-box helicases possessing all three Vasa-defining peripheral domains, and they share redundancy in maintaining the germline. *glh-1* null mutants remain fertile at 20°C, displaying minor defects in sperm activation and germline expression, but at 26°C lose fertility, showing reduced germ cells and often lacking sperm (Rochester et al., 2022; Spike et al., 2008). *glh-2* null mutants show wild-type fertility at 20°C and 26°C (Spike et al., 2008). In contrast, *glh-2 glh-1* double mutants lose fertility at both 20°C and 26°C (Marnik et al., 2019). The redundancy among GLH proteins enables the evaluation of domain-specific contributions to germline development in fertile and living animals. Precision edits of endogenous *glh-1* show that disrupting any of the three Vasa-defining peripheral domains induces temperature-sensitive sterility, suggesting that the peripheral domains of GLH-1 can be as important to germline development as its helicase activity (Marnik et al., 2019).

In this study, we used a yeast-two-hybrid (Y2H) screen to complement previous approaches in identifying GLH-1-interacting proteins. An earlier Y2H screen used only the helicase domain of GLH-1 as bait, potentially missing crucial interactions with Vasa-defining peripheral domains (Smith et al., 2002). Here, we used full-length GLH-1, to identify BYN-1, the *C. elegans* homolog of bystin, as one of six high-confidence interactions. Curiously, GLH/Vasa/DDX4 is found in cytoplasmic germ granules, whereas bystin is typically found in the nucleolus where it is involved in 40S ribosomal subunit assembly (Fukuda et al., 2008; Miyoshi et al., 2007; Roos et al., 1997). However, bystin's localization can also be dynamic. For instance, under nucleolar stress in human cancer cell lines, bystin mobilizes from the nucleolus into the cytoplasm (Ayala et al., 2006; Miyoshi et al., 2007). Bystin (*Bysl*) mRNA expression in the mouse is upregulated in activated early embryo blastocysts (Aoki et al., 2006; Hamatani et al., 2004). During embryonic implantation in humans, bystin is expressed in the trophectoderm and interacts with a protein called trophinin in the cytoplasm. This interaction modulates epidermal growth factor receptor activation, stimulating the epithelial-to-mesenchymal transition of trophectoderm into syncytiotrophoblasts that can invade the uterine wall (Fukuda and Nozawa, 1999; Fukuda and Sugihara, 2008; Nakayama et al., 2003; Sugihara et al., 2007, 2008; Suzuki et al., 1998). Disruption of bystin in mice results in embryonic lethality soon after implantation (Aoki et al., 2006), leaving the molecular and developmental mechanisms of cytoplasmic bystin–trophinin interactions unresolved. Interestingly, GLH-1 in *C. elegans* and trophinin in placental mammals have very similar decapeptide phenylalanine-glycine (FG)-repeat domains, suggesting potential sites of interaction with BYN-1/bystin in the cytoplasm.

Here, we show that BYN-1 and GLH-1 are subcellularly partitioned from each other through most of *C. elegans* germline

Davis Center for Regenerative Biology and Aging, The Mount Desert Island Biological Laboratory, Bar Harbor, ME 04672, USA.
*Present address: Department of Bioscience and Biotechnology, Konkuk University, Seoul 05029, Republic of Korea.

‡Author for correspondence (dupdike@mdibl.org)

H.M., 0000-0001-9691-770X; E.L.S., 0000-0001-9680-6348; C.S.S., 0000-0002-8459-1084; D.L.U., 0000-0002-1745-3669

Handling Editor: Swathi Arur
Received 8 January 2024; Accepted 2 August 2024

Development (2024) 151, dev202694. doi:10.1242/dev.202694

development. The two proteins ultimately colocalize when BYN-1 is redistributed during nucleolar breakdown in spermatocytes towards the end of meiotic prophase, when it leaves the nucleus to reassemble in GLH-1-containing perinuclear germ granules. The interaction between GLH-1 and BYN-1 persists through spermatogenesis and cues the CED-1-dependent uptake of anucleate residual bodies (RBs) by overlying gonadal epithelial sheath cells. Although the extent to which RB uptake resembles cellular infiltration in cancer or human embryonic implantation has yet to be determined, our results implicate BYN-1 in a cellular uptake signaling cascade the genetics of which can be illuminated in *C. elegans*.

RESULTS

BYN-1 identified as a binding partner with *C. elegans* GLH-1

To investigate the roles of GLH-1 and its binding partners in regulating germ cell development, we analyzed 80,000,000 potential interactions in a Y2H screen using full-length GLH-1 as bait. BYN-1, the ortholog of human BYSL (bystin like), was one of six high-confidence interactions identified, appearing in six sequenced clones (Fig. 1A, Table S1). Bystin is evolutionarily conserved from yeast to humans (Fig. S1A). In *Saccharomyces cerevisiae*, *Drosophila*, HeLa cells, COS-7 cells, mouse embryo, and mouse embryonic stem cells, bystin homologs are mainly nucleolar, with roles in 18S ribosomal RNA and 40S subunit assembly (Adachi et al., 2007; Miyoshi et al., 2007; Roos et al., 1997; Stewart and Nordquist, 2005). Bystin is cytoplasmic in human trophoblasts, forming a complex with the cell adhesion molecule trophinin to mediate the initial attachment of the blastocyst to uterine epithelial cells during implantation (Sugihara et al., 2007; Suzuki et al., 1998). *C. elegans* does not have a homolog of trophinin, but GLH-1 and trophinin share a unique and strikingly similar glycine-rich decapeptide FG-repeat domain (Fig. 1B, Fig. S1B,C).

The FG-repeat domains of GLH proteins help distribute germ granules around the nuclear periphery by tethering to peripheral FG nucleoporins (FG-Nups) (Updike et al., 2011). Removing the FG-repeats from GLH-1 and GLH-2 interferes with the wetting-like distribution of these proteins around the nuclear periphery of primordial germ cells, resulting in germ granules that are still attached but less evenly distributed and larger and more spherical in shape (Marnik et al., 2019). A directed 1×1 Y2H assay was used to determine whether the interaction with BYN-1 is mediated through the FG-repeat domain of GLH-1 (Fig. 1C). This assay confirmed that the C-terminus of BYN-1 (aa 372-449) interacts with full-length GLH-1 (Fig. 1C, column 4) and GLH-1 ΔFG, which is missing 15 of its 19 FG-repeats from the N terminus (Fig. 1C, column 8). Increasing amounts of 3-aminotriazole, an inhibitor of the HIS3 Y2H reporter, showed that the strength of this interaction is severely compromised with the removal of these FG-repeats. However, the Y2H assay also showed that these 15 FG-repeats are not sufficient to bind BYN-1 alone (Fig. 1C, column 6). These data suggest that other GLH-1 domains are likely required to seed contact with BYN-1, but that the FG-repeat domain stabilizes the interaction.

BYN-1 is essential for *C. elegans* fertility and development

Large-scale RNA interference (RNAi) screens in *C. elegans* have shown that BYN-1 is essential. Depletion of *byn-1* mRNA causes phenotypes ranging from embryonic lethality, larval arrest, sterility,

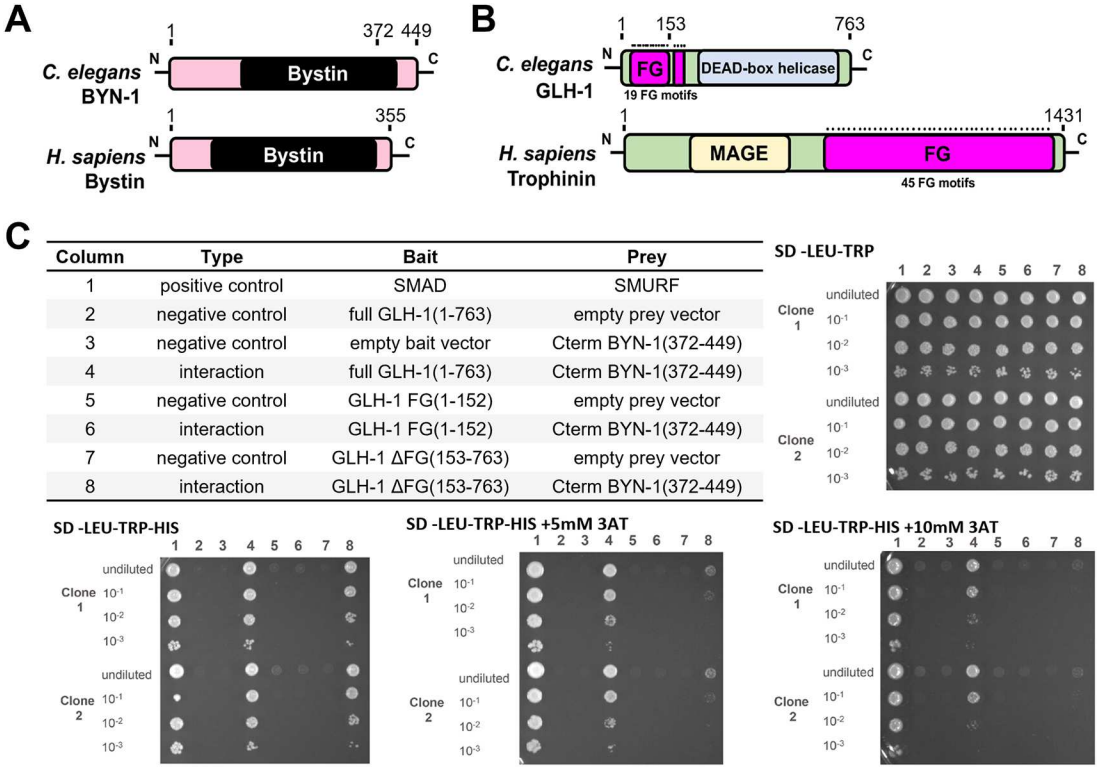

Column	Type	Bait	Prey
1	positive control	SMAD	SMURF
2	negative control	full GLH-1(1-763)	empty prey vector
3	negative control	empty bait vector	Cterm BYN-1(372-449)
4	interaction	full GLH-1(1-763)	Cterm BYN-1(372-449)
5	negative control	GLH-1 FG(1-152)	empty prey vector
6	interaction	GLH-1 FG(1-152)	Cterm BYN-1(372-449)
7	negative control	GLH-1 ΔFG(153-763)	empty prey vector
8	interaction	GLH-1 ΔFG(153-763)	Cterm BYN-1(372-449)

Fig. 1. BYN-1 is identified as a binding partner of GLH-1. (A) Schematic of bystin/BYN-1 proteins in *C. elegans* and *Homo sapiens*, with the bystin coiled-coil domain indicated in black. (B) Schematic of the conserved FG domain in *C. elegans* GLH-1 and *H. sapiens* trophinin. FG, phenylalanine-glycine repeats (black dots represent FG-repeats); MAGE, melanoma antigen gene domain. (C) Directed 1×1 Y2H assay shows that the C terminus of BYN-1 binds full-length GLH-1, but the FG-repeat domain of GLH-1 is not sufficient to bind BYN-1. Removal of the FG-repeat domain from GLH-1 weakens binding to BYN-1 when stringency is challenged with increasing concentrations of 3-aminotriazole (3AT).

Development (2024) 151, dev202694. doi:10.1242/dev.202694

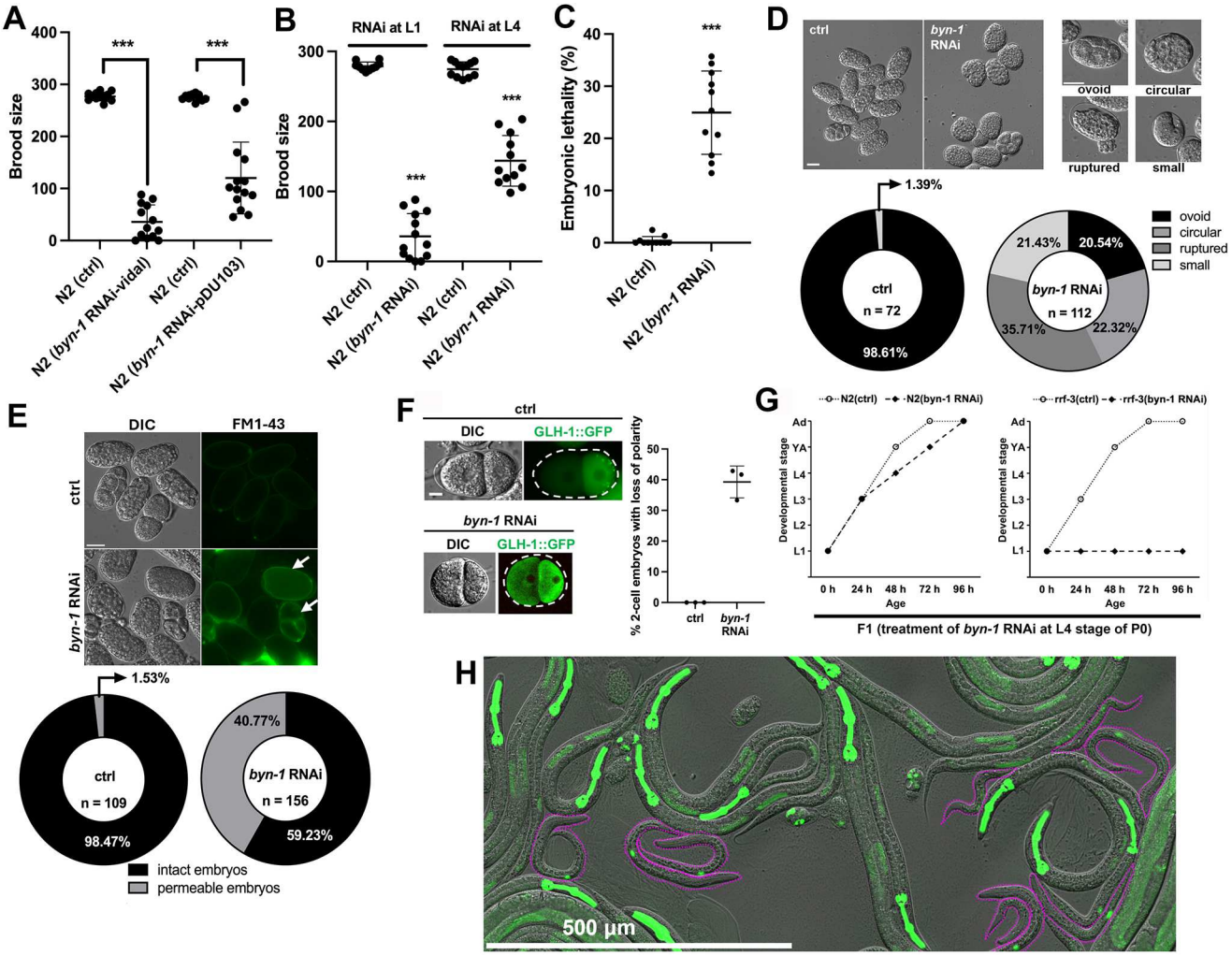

Fig. 2. BYN-1 affects cell polarity and migration and is essential for fertility and development. (A) Brood size comparison of wild-type N2 L1 worms fed control RNAi (L4440; ctrl) or RNAi targeting *byn-1* (Vidal *byn-1* RNAi clone, pDU103 *byn-1* N-terminal RNAi clone). Number of analyzed animals: *n*=14 for N2 (ctrl), *n*=14 for N2 (*byn-1* RNAi-Vidal), *n*=12 for N2 (ctrl), *n*=14 for N2 (*byn-1* RNAi-pDU103). (B) Brood size comparison of wild-type N2 L1 and L4 worms fed control RNAi (L4440) or *byn-1* RNAi (Vidal). Number of analyzed animals: *n*=12 for the respective conditions. (C) Embryonic lethality from wild-type N2 L4 worms fed control RNAi (L4440) or *byn-1* RNAi (Vidal). Number of analyzed mothers: *n*=12 for N2 (ctrl), *n*=11 for N2 (*byn-1* RNAi). (D) DIC images of embryos from the dissected wild-type adults that had been fed control (L4440) or *byn-1* RNAi (Vidal) at L4 stage. Embryos were classified into four categories: (1) ovoid, (2) circular, (3) ruptured or (4) small. Scale bars: 20 µm. (E) The eggshells of progeny from L4 animals fed *byn-1* RNAi, but not control RNAi, are permeable to the lipophilic dye FM1-43 (arrows). Scale bar: 20 µm. *n*=number of embryos. (F) Depletion of *byn-1* in L4 animals causes abnormal GLH-1::GFP localization in live embryos. Scale bar: 10 µm. Graph shows the percentage of two-cell embryos with loss of GLH-1 polarity caused by depletion of *byn-1*. Number of analyzed two-cell embryos: *n*=34 for ctrl, *n*=38 for *byn-1* RNAi. (G) The developmental stage of the F1 generation from L4 stage worms fed control or *byn-1* RNAi every 24 h at 20°C. Ad, adult (with embryos); YA, young adult (with no embryos). Number of analyzed animals: *n*=60 for N2 (ctrl), *n*=62 for N2 (*byn-1* RNAi), *n*=50 for *rrf-3* (ctrl), *n*=66 for *rrf-3* (*byn-1* RNAi). (H) F1 progeny from CRISPR-generated *glh-1*::GFP I; Δ*byn-1* III hermaphrodites balanced over *hT2 g*(*qIs48*-green pharynx) I/III, 3 days post-egg-lay. Δ*byn-1* homozygous animals (no green pharynx) are outlined in magenta and show fully penetrant primordial germ cell (*glh-1*::GFP) and L1 arrest phenotypes. In A-C,F, error bars represent s.d. ***P<0.001 (two-tailed, unpaired Student's t-test).

and aberrant germline development (Green et al., 2011, 2024; Kamath et al., 2003; Rual et al., 2004; Sönnichsen et al., 2005; Sun et al., 2011). We confirmed these phenotypes using two different *byn-1* RNAi feeding constructs, one from the Vidal ORFeome-based RNAi library (Rual et al., 2004) and another directed at the *byn-1*-specific sequence in its N terminus (Fig. 2A). Closer examination revealed a drastic reduction in the brood size of adult animals subjected to *byn-1* RNAi feeding in the first larval stage (L1) (Fig. 2B). When *byn-1* RNAi feeding was initiated in the fourth larval stage (L4), brood sizes in that generation were still reduced (Fig. 2B), which may reflect a decrease in germ cell proliferation (Fig. S2A) and an alteration in physiological apoptosis at 48 h post-L4 stage (Fig. S2B,C). Embryonic progeny of these *byn-1* RNAi-treated nematodes exhibited increased lethality (Fig. 2C), were often ruptured or misshapen (Fig. 2D), and showed permeability defects (Fig. 2E). *byn-1* RNAi embryos also showed defects in GLH-1 partitioning to P blastomeres (Fig. 2F), developmental delays in hatched progeny, and L1-arrested development of hatched progeny in the RNAi-sensitive *rrf-3* mutant background (Fig. 2G). To assess the null phenotype, CRISPR gene editing was used to create a precise *byn-1* deletion over a balancer chromosome marked with myo-2::GFP (pharynx fluorescence). Homozygous animals carrying the *byn-1* deletion (no green pharynx) arrested in the first larval stage, as determined by size and the GLH-1::GFP pattern (Fig. 2H). In yeast, the BYN-1 homolog has been shown to be essential for 18S rRNA production for 40S subunit assembly (Roos et al., 1997). The L1

Development (2024) 151, dev202694. doi:10.1242/dev.202694

arrest we observed is identical to mutant phenotypes of other *C. elegans* genes required for 18S rRNA and 40S subunit assembly and translation (Curran and Ruvkun, 2007; Dalton and Curran, 2018; Hansen et al., 2007; Pan et al., 2007; Saijou et al., 2004), suggesting a similar role for BYN-1 in 40S subunit synthesis.

Endogenous BYN-1 is partitioned away from GLH-1 until spermatogenesis

To determine the subcellular localization of BYN-1 and where it might overlap with GLH-1, CRISPR/Cas9 was used to place a C-terminal mCherry::V5 tag on endogenous BYN-1 in a strain in which endogenous GLH-1 was tagged with GFP::3xFLAG (S3A). BYN-1 was expressed in most cell types of adult hermaphrodites and males (Fig. S3B), and the tag presented no deleterious effects on fertility or development (Fig. S3C,D). Live imaging of germ cells showed BYN-1::mCherry::V5 in the nucleus and enriched in nucleoli, partitioned away from GLH-1 residing on the cytoplasmic surface of the nuclear periphery (Fig. 3A, Fig. S4A,B). The partitioning of BYN-1::mCherry::V5 from GLH-1::GFP::3xFLAG is seemingly at odds with the Y2H results. However, during spermatogenesis, the nucleolus breaks down in the condensation zone during late diplotene (Shakes et al., 2009). At this stage, we observed BYN-1 to disperse throughout the nucleoplasm and then enter the cytoplasm at the karyosome stage of spermatogenesis, where it colocalized with GLH-1 (Fig. 3B,C). A putative monopartite nuclear localization signal (EKQKRKR) is found within the disordered N terminus of BYN-1, but a putative nuclear export sequence was not evident. Therefore, the entry of BYN-1 into the cytoplasm may require the initiation of nuclear envelope breakdown. Unlike in spermatogenesis, nucleoli remain intact throughout the diplotene and early diakinesis stages of oogenesis, when BYN-1 remains in the nucleolus (Fig. 3D, Fig. S4B). BYN-1 also colocalized with GLH-1 in L4 hermaphrodites as germ cells entered spermatogenesis (Fig. S4C). BYN-1 and GLH-1 remained colocalized throughout meiotic divisions until both proteins were finally packaged into the RB upon spermatid budding (Fig. 3E). These RBs are then engulfed and cleared out by the surrounding somatic gonad. Neither GLH-1 nor BYN-1 was observed in spermatids. This narrow spatiotemporal window of interaction, as evidenced by the Y2H results, likely explains why BYN-1 does not substantially co-immunoprecipitate with GLH-1 in adult hermaphrodite lysates (Fig. S5) and why BYN-1 was not identified in previous GLH-1 immunoprecipitation-qMS experiments

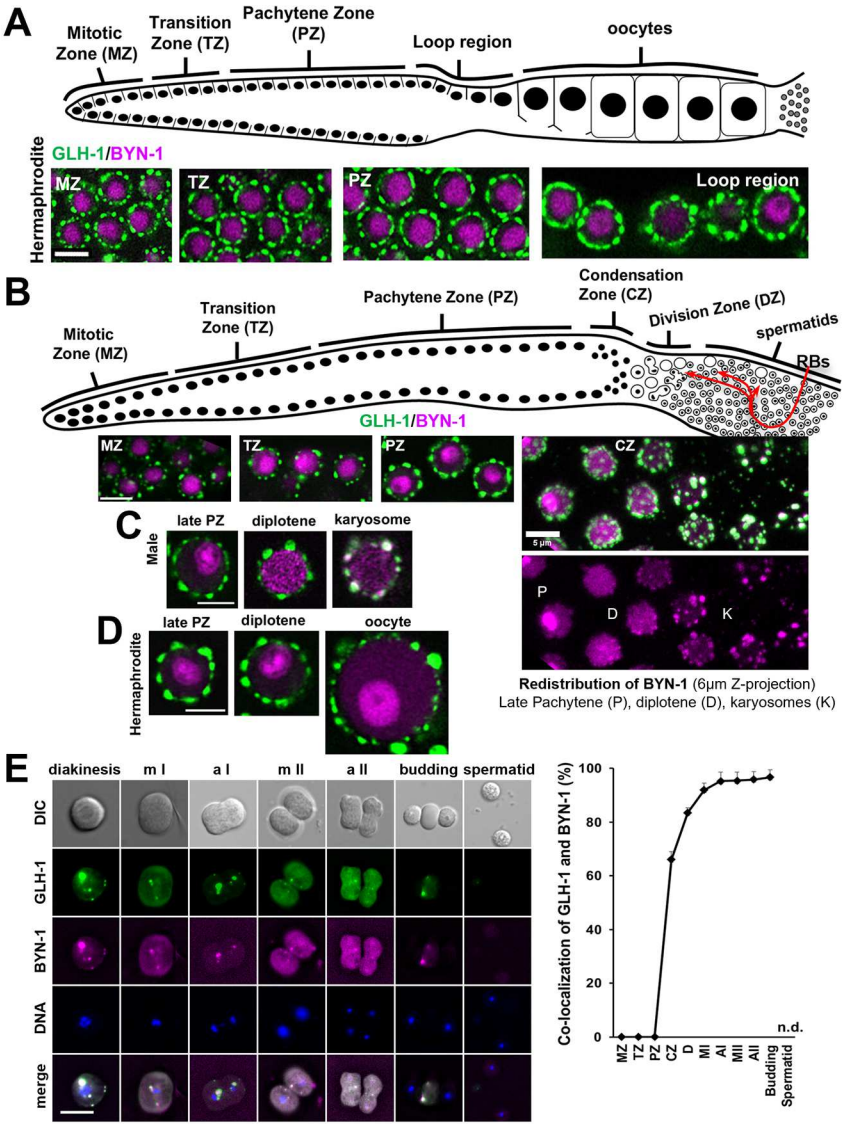

Fig. 3. BYN-1 and GLH-1 localization in germ cells. (A) Top: Schematic of a hermaphrodite gonad arm in *C. elegans* adults. In the gonad arm, germ cells undergo mitotic proliferation in the distal 'mitotic zone' (MZ). During their passage through the 'transition zone' (TZ), germ cells stop dividing and initiate meiosis. Germ cells in meiotic prophase I accumulate in the 'pachytene zone' (PZ). The 'loop region' is the anatomic bend in the gonad. The more proximal region of the gonad arm is filled with developing oocytes. Bottom: Confocal live images showing BYN-1::mCherry and GLH-1::GFP during oogenesis in adult hermaphrodites (20°C). GLH-1 is located on the cytoplasmic surface of the nuclear periphery, and BYN-1 is in the nucleolus during oogenesis. Scale bar: 5 µm. (B) Top: Schematic of a male gonad arm in *C. elegans* adults. Following an extended pachytene stage, spermatocytes enter the karyosome stage in the condensation zone (CZ) before detaching from the syncytial germline. Meiotic divisions in the division zone (DZ) are followed by spermatids budding from anucleate residual bodies (RBs) that become engulfed and cleared by the somatic gonad surrounding the seminal vesicle. Bottom: Confocal live images showing the dynamic localization of BYN-1::mCherry and GLH-1::GFP in germ cells from adult males (20°C). BYN-1 is nucleolar from MZ to PZ but translocates into the cytoplasm at CZ to colocalize with GLH-1. The MZ, TZ and PZ panels represent a single confocal plane, whereas the CZ panels represent a maximum-intensity *z*-projection to capture the change in BYN-1 dynamics. Scale bars: 5 µm. (C) Enlarged confocal live images of GLH-1 and BYN-1 in respective germ cell stages of male germline. Scale bar: 3 µm. (D) Enlarged confocal live images of GLH-1 and BYN-1 in respective germ cell stages of hermaphrodite germline. Scale bar: 3 µm. (E) Representative live images of GLH-1 and BYN-1 in dissected male germ cells during the meiotic and post-meiotic events of spermatogenesis. The graph shows the percentage of colocalization of GLH-1 and BYN-1 among cells in respective stages of spermatogenesis (n=30 per stage). Error bars represent s.d. AI/AII, anaphase I/II; D, diplotene; MI/MII, metaphase I/II; n.d., no data.

Development (2024) 151, dev202694. doi:10.1242/dev.202694

(Marnik et al., 2019), but is able to physically bind GLH-1 when in the same cellular compartment.

BYN-1 contributes to residual body clearance

To investigate further the role of BYN-1 in spermatogenesis, the stage at which BYN-1 and GLH-1 colocalize, we used RNAi to knock down *byn-1* in L1-staged males and examined their DNA as adults by DAPI staining (Fig. 4, Fig. S6). Compared with control (empty L4440 vector RNAi), *byn-1* RNAi males showed similar spermatogenic developmental zones and produced mature spermatids (Fig. 4A). However, GLH-1::GFP expression looked markedly different following *byn-1* RNAi. GLH-1 is deposited in

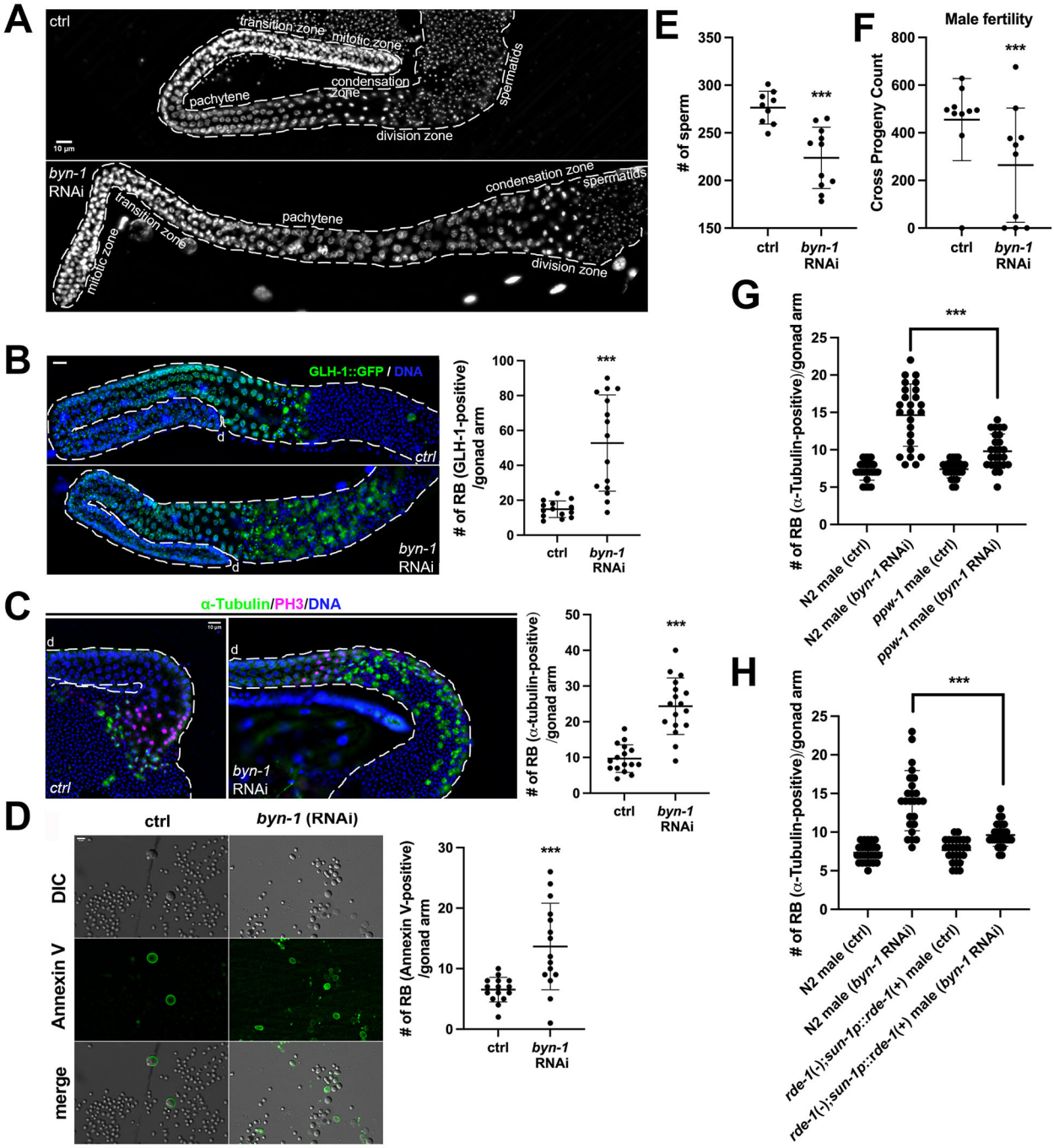

Fig. 4. BYN-1 contributes to the clearance of RBs during spermatogenesis. (A) DAPI-stained adult male dissected gonads labeled by developmental stages. Scale bar: 10 µm. (B) GLH-1::GFP expression in control (ctrl) RNAi and *byn-1* RNAi-treated adult stage males. Male gonads were fixed and counterstained with DAPI (blue). Scale bar: 10 µm. d, distal region of the gonad. Graph shows the number of GLH-1 containing RBs in each male gonad. *n*=14 for ctrl, *n*=15 for *byn-1* RNAi. (C) Dissected gonads from wild-type control and *byn-1* RNAi males co-stained with anti-α-tubulin (green), anti-phosphorylated histone H3 Ser10 (magenta), and DAPI (blue). Scale bar: 10 µm. d, distal region of the gonad. Graph shows the number of α-tubulin-positive RBs at the proximal region of gonad. *n*=16 for ctrl, *n*=17 for *byn-1* RNAi. (D) Representative live images of dissected sperm showing that RBs stain with Annexin V (green). Graph shows the number of Annexin V-positive RBs. *n*=15 for ctrl, *n*=15 for *byn-1* RNAi. Scale bar: 10 µm. (E) Sperm numbers were quantified in males of each group. *n*=9 for ctrl, *n*=11 for *byn-1* RNAi. (F) Cross progeny counts from *fog-2* females mated with control RNAi and *byn-1* RNAi males. *n*=10 for ctrl, *n*=10 for *byn-1* RNAi. (G,H) RB (α-tubulin positive) counts in the proximal region of dissected male gonads. *n*=25 for the respective conditions. Error bars represent s.d. Statistical significance was calculated using a two-tailed, unpaired Student's *t*-test ***P<0.001.

Development (2024) 151, dev202694. doi:10.1242/dev.202694

RBs upon spermatid budding and lost when RBs are cleared by engulfment from the surrounding somatic gonad (Huang et al., 2012). Following *byn-1* RNAi, GLH-1::GFP positive RBs accumulated, pointing to defects in RB clearance (Fig. 4B). To confirm this observation, control and *byn-1* RNAi males were co-immunostained with anti-phosphohistone (pH3) antibody (which marks late G2 and M phases) and anti-α-tubulin antibody (which marks spindle microtubules later deposited in RBs). The expression of pH3-positive cells in *byn-1* RNAi animals was normal; however, RBs positive for α-tubulin were significantly increased in the post-meiotic spermatid region in *byn-1* RNAi males (Fig. 4C). To confirm RB accumulation in *byn-1* RNAi males, we dissected out sperm and stained with Annexin V, which is known to bind the phosphatidylserine (PS) expressed on the surface of RBs that serves as an 'eat me' signal for clearance (Huang et al., 2012). We observed an increase in RBs, all of which were Annexin-V positive, demonstrating that the PS uptake signal is present in *byn-1* RNAi males but the RBs are not being engulfed (Fig. 4D). These results suggest that BYN-1 functions in RB clearance during spermatogenesis in *C. elegans* downstream of the PS 'eat me' signal. It has been reported that RB accumulation affects sperm counts and male mating efficiency (Huang et al., 2012). Indeed, compared with the control at 8 h post-L4 stage, the number of sperm in *byn-1* RNAi males was significantly reduced (Fig. 4E). This reduction in sperm number was accompanied by a reduction in the mating efficiency of *byn-1* RNAi males with *fog-2* females (Fig. 4F). We further tested whether the abnormal RB phenotype is caused by BYN-1 in the germline or soma. We observed the RB phenotype for *byn-1* using soma or germline-biased RNAi strains. RNAi depletion of *byn-1* in both germline and soma-biased strains increased RB accumulation, but significantly less than in the wild-type background (Fig. 4G,H). These results suggest that RB uptake requires BYN-1 in the germline, but may also require cooperation of BYN-1 in both germline and soma. Taken together, we conclude that BYN-1 affects sperm counts and male mating efficiency by ensuring the clearance of RBs in the seminal vesicle.

BYN-1 acts as an upstream regulator of CED-1 during RB clearance

There are five sheath cell pairs surrounding each gonadal arm in hermaphrodites that serve as phagocytic cells for clearing germ cell corpses during oogenesis (Gumienny et al., 1999). The gonadal sheath cells are also the main phagocytic cells that clear RBs during spermatogenesis (Huang et al., 2012). CED-1 is a transmembrane scavenger-receptor-like protein homologous to mammalian LRP1 and MEGF10, expression of which in gonad sheath cells triggers the clearance of RBs in both hermaphrodites and males. The ABC transporter CED-7, which clusters around cell corpses that are recognized by CED-1, is thought to be dispensable for RB clearance in males, whereas the parallel CED-12 pathway plays a more minor role in RB clearance (Fig. 5A) (Huang et al., 2012). To understand how BYN-1 regulates RB clearance during spermatogenesis, we observed hermaphrodites, in which RB clearance occurs during a limited time window as the germline switches from sperm to oocyte production (Fig. 5B). A CED-1::GFP transgene readily labels cells of the somatic gonad as they engulf RBs (Fig. 5C). Compared with the control, *byn-1* RNAi significantly reduced CED-1::GFP-positive cells surrounding the RBs in 6 h post-L4 animals (Fig. 5C,D). In adults (24 h post-L4), some CED-1 positive cells persisted near the spermatheca of *byn-1* RNAi animals (Fig. 5C, white arrows; Fig. 5E), but in the loop region, where physiological apoptosis occurs, the number of CED-1 positive cells was similar between *byn-1* and control RNAi in 24 h post-L4 stage hermaphrodites (Fig. S7). These results suggest that CED-1-mediated engulfment is not increased in more distal germ cells where BYN-1 is nucleolar. Rather, CED-1-mediated engulfment increases when BYN-1 is cytoplasmic during RB clearance. *byn-1* RNAi was performed in both *ced-1* and *ced-12* mutant backgrounds, in which the accumulation of RBs shows that their clearance is compromised. *byn-1* RNAi did not further enhance RB accumulation over the control in these backgrounds (Fig. 5F-H). We also observed that the number of RBs surrounded by CED-1::GFP in males was significantly reduced by *byn-1* RNAi (Fig. S8), consistent with the decrease in CED-1 activity caused by *byn-1* RNAi in hermaphrodites. We further investigated whether sperm from *byn-1* RNAi-treated males are fully functional or whether they exhibit other defects. Upon *in vitro* sperm activation with pronase, a subtle but significant decrease in pseudopod length was observed (Fig. S9). This result suggests that BYN-1 may also play a role in spermiogenesis. Altogether, these results suggest that BYN-1 contributes to RB clearance upstream of the transmembrane engulfment receptor CED-1.

FG-repeat domains in GLH proteins function with BYN-1 to clear RBs

The FG-repeats of *C. elegans* GLH-1 are most similar to the FG-repeats of the bystin-interacting protein trophinin (Fig. S1B; Suzuki et al., 1998). Trophinin-like FG-repeats are also found in the germ-granule proteins GLH-2, GLH-4, RDE-12 and DDX-19 (Sheth et al., 2010). We have previously shown the impact on germ granule size and shape when FG-repeat domains are deleted from GLH-1 (ΔFG) and both GLH-1 and GLH-2 (2ΔFG) (Fig. 6A; Marnik et al., 2019). 2ΔFG animals have reduced broods compared with wild type, but to a lesser extent than observed with *byn-1* RNAi (Fig. S10A). To determine whether the FG-repeats of GLH-1 and GLH-2 help facilitate RB uptake, RB accumulation was quantified in wild-type, ΔFG and 2ΔFG animals. At both 6 and 24 h post-L4, 2ΔFG hermaphrodites showed a significant accumulation of RBs compared with the control (Fig. 6B). This increase in RB accumulation was accompanied by a significant decrease in the number of sperm (Fig. 6C). These results suggest that the FG-repeat domains of GLH-1 and GLH-2 contribute to RB clearance.

We observed that RB accumulation is higher with *byn-1* RNAi than it is in 2ΔFG animals. This difference in accumulation may be due to the presence of other perinuclear FG-repeat proteins or the ability of BYN-1 to bind elsewhere on GLH-1 or GLH-2, using the FG-repeats to stabilize the association. However, RB accumulation in *byn-1* RNAi animals was not enhanced by the 2ΔFG background, suggesting that the FG-repeats of GLH-1 and GLH-2 act in the same pathway as BYN-1 for RB clearance (Fig. 6D). The same conclusion can be drawn when comparing the decrease in sperm (Fig. 6E). 2ΔFG animals showed reduced colocalization between GLH-1 and BYN-1 during spermatogenesis (Fig. 6F,G), suggesting that the efficient clearance of RBs requires BYN-1 to interact with the FG-repeats of GLH proteins in these cytoplasmic foci. We also observed that the size of GLH-1::GFP granules within the condensation zone was markedly increased in 2ΔFG animals compared with the wild type (Fig. 6H), reflecting the size increase previously reported in 2ΔFG embryos (Chen et al., 2020; Marnik et al., 2019). Within RBs, BYN-1 intensity and colocalization with GLH-1 were reduced in 2ΔFG mutants compared with wild type (Fig. 6I-K). These data suggest that, in RBs, BYN-1 is stabilized by FG-repeat interactions within GLH assemblies, perhaps to cue CED-1-dependent uptake of the RBs by the surrounding somatic gonad.

Development (2024) 151, dev202694. doi:10.1242/dev.202694

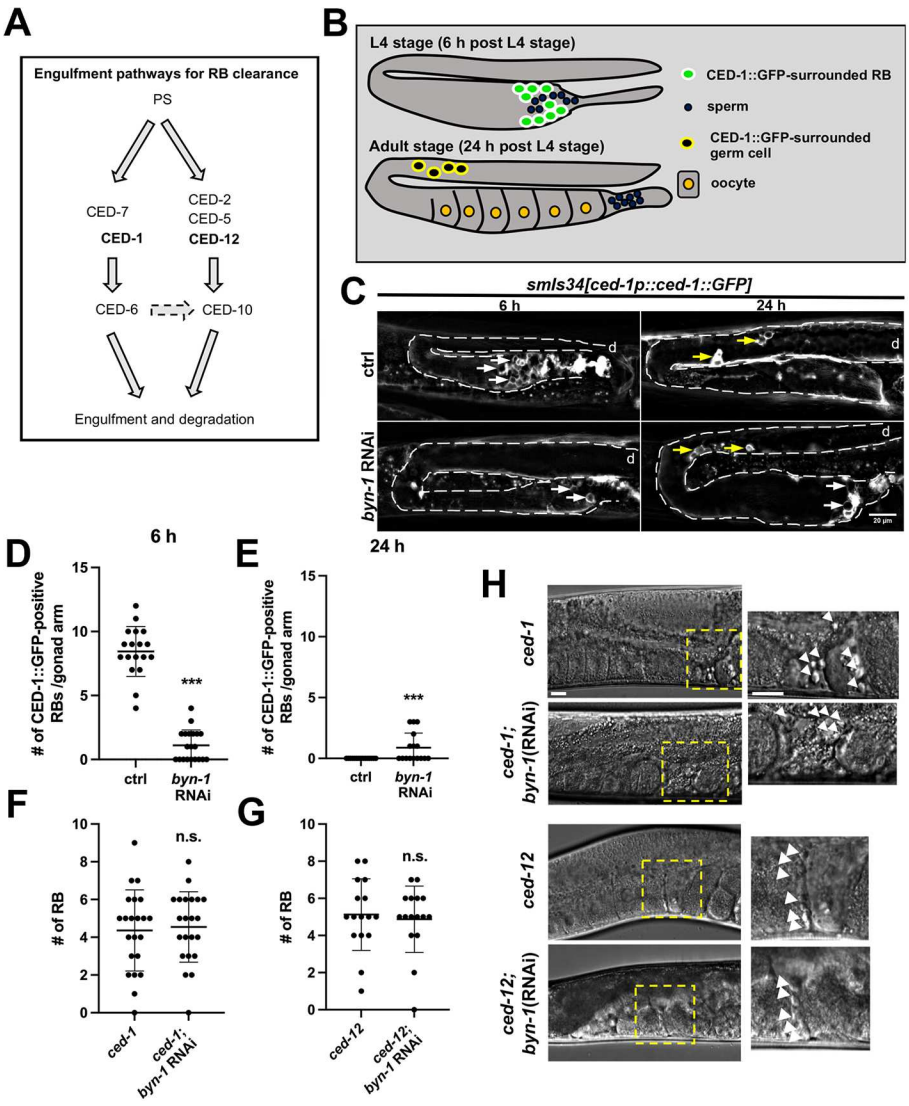

Fig. 5. BYN-1 functions upstream of CED-1 during RB clearance. (A) Engulfment pathways for RB clearance during spermatogenesis as described by Huang et al. (2012). PS, phosphatidylserine. (B) Schematic of a gonad arm in *C. elegans* L4-larval-stage to adult hermaphrodite. In the L4 stage, RBs at the proximal region of the gonad are surrounded by CED-1 (green circle with white border), a transmembrane receptor that mediates cell corpse engulfment and clearance of RBs during spermatogenesis. In adults, apoptotic germ cells are mostly observed in the late pachytene zone surrounded by CED-1 (black circle with yellow border) during oogenesis. (C) RB engulfment visualized with *smIs34[ced-1p::ced-1::GFP]* transgene at 20°C. Engulfed RBs surrounded by CED-1::GFP are marked with white arrows. Yellow arrows mark the engulfment of germ cell corpses. *byn-1* RNAi adult animals showed both engulfed RBs at the proximal region of the gonad and engulfed germ cell corpses at the pachytene zone. d, distal region of gonad. Scale bar: 20 µm. (D,E) The number of RBs surrounded by CED-1::GFP per gonad arm at 6 h and 24 h post-L4 stage at 20°C. ctrl, control. *n*=18-20 for the respective conditions. (F,G) The number of RBs, as determined by DIC microscopy (H), in either *ced-1(e1735)* or *ced-12 (n3261)* hermaphrodites 24 h post-L4 stage. *n*=16-22 for the respective conditions. (H) DIC images of RB retention in the spermatheca of 24 h post-L4 stage *ced-1* and *ced-12* hermaphrodites. Yellow dashed boxes indicate the approximate region that is enlarged to the right. Arrowheads represent RBs. Scale bar: 10 µm. Error bars represent s.d. Statistical significance was calculated using a two-tailed, unpaired Student's *t*-test. ***P<0.001. n.s., not significant (P>0.05).

To analyze further the dependence of the RB accumulation phenotype on GLH FG-repeats, we examined RB accumulation in animals carrying *glh-1* and *glh-2* temperature-sensitive sterile alleles that still retain their FG-repeat domains (Marnik et al., 2019). One of these strains carries a mutation that deletes the zinc-finger domain from GLH-1 but leaves its association with germ granules intact. A second strain carries a T-to-A mutation in the C-terminal helicase of GLH-1 (aa 663) to inhibit its ATPase activity, dispersing GLH-1 into the cytoplasm. The third strain carries E-to-A mutations in the DEAD-box of both GLH-1 and GLH-2 that disperses them into the cytoplasm and likely inhibits their helicase activity. RB accumulation phenotypes were not observed in these three strains (Fig. S10B,C), pointing to the significance of BYN-1–FG-repeat interactions for RB clearance during spermatogenesis.

DISCUSSION

BYN-1-mediated engulfment is dependent on its subcellular location

The phenotypic analysis of *byn-1* RNAi animals suggests that the activity of BYN-1 in the nucleolus is crucial for cell proliferation and survival, whereas its activity in the cytoplasm mediates cell engulfment. These observations provide added insight into a dual function for BYN-1. By imaging cells in live animals, the localization and expression of BYN-1 during germline differentiation revealed previously unseen dynamic processes that drive RB clearance during spermatogenesis. BYN-1 is localized in the nucleus and enriched in nucleoli, partitioned away from GLH-1 and the FG-repeat-rich germ granules residing on the cytoplasmic surface of the nuclear envelope (Fig. 7A). In the diplotene stage of spermatogenesis, as nucleoli disassemble, BYN-1 first disperses throughout the nucleoplasm and then enters the cytoplasm where it encounters GLH-1. As spermatids are formed, BYN-1 and GLH-1 are partitioned into anucleate RBs and engulfed by the surrounding somatic gonad. The correlation of these activities suggests that the translocation of BYN-1 and colocalization with FG-repeat domain-containing GLH proteins triggers cell engulfment.

For comparison, during oogenesis nucleoli remain intact through the diplotene stage and do not disassemble until the end of diakinesis. As a result, nucleolar BYN-1 is retained in maturing oocytes until after most germ granules disperse. In addition, the activity of CED-1 was not significantly affected by the depletion of *byn-1* during physiological apoptotic events in oogenesis. These results suggest that BYN-1 does not function in cell migration and engulfment while it is retained in nucleoli. Therefore, BYN-1-mediated engulfment is likely dependent on its subcellular location. BYN-1 does not appear to encounter GLH-1 during oogenesis as it does during spermatogenesis. It will be

Development (2024) 151, dev202694. doi:10.1242/dev.202694

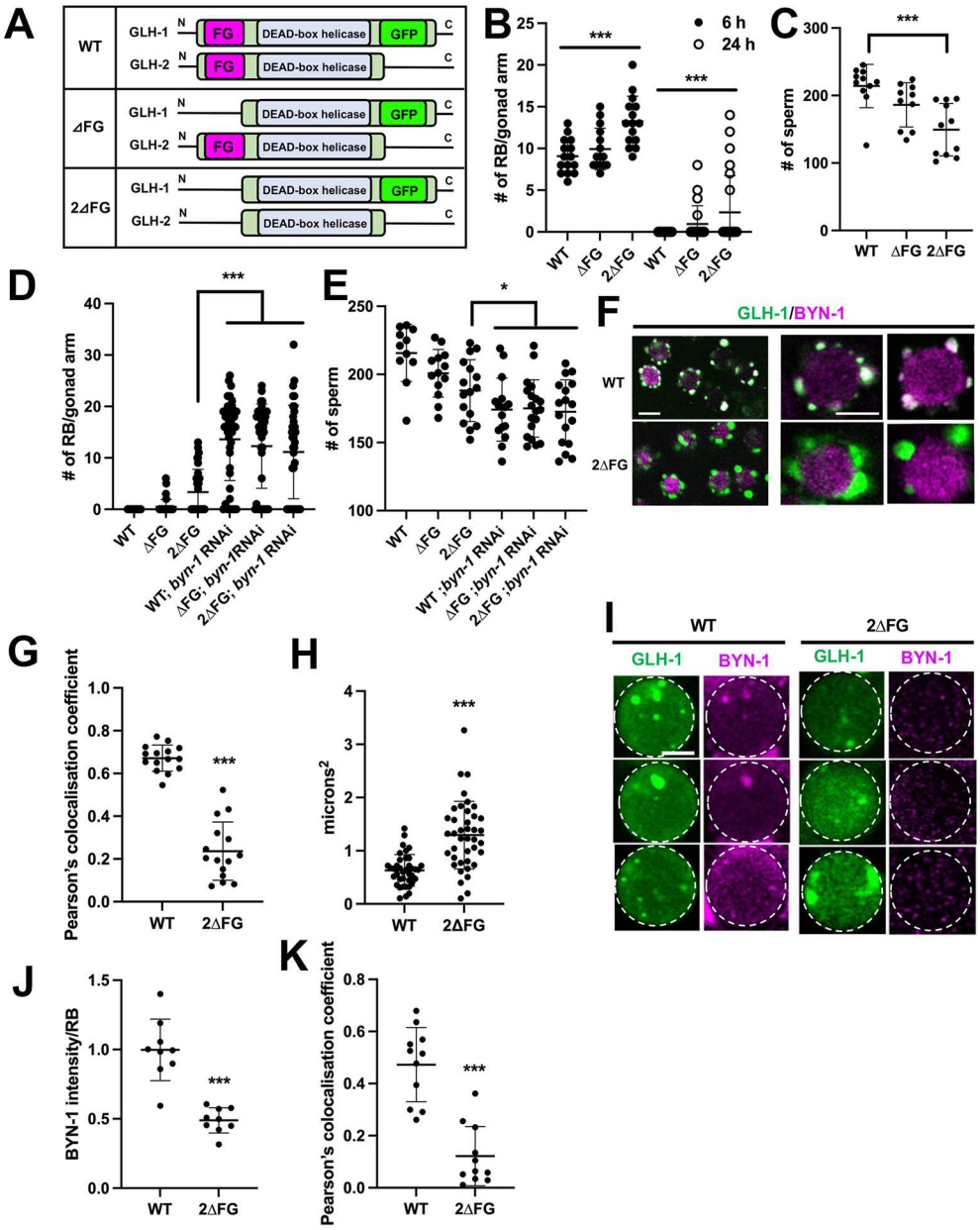

Fig. 6. The FG-repeat domains of GLH-1 and GLH-2 contribute to RB clearance. (A) Schematic of endogenous GLH-1::GFP and GLH-2 modified proteins in wild-type (WT), ΔFG and 2ΔFG background strains. (B) GFP-expressing RBs were scored 6 h or 24 h post-L4 stage in hermaphrodites. *n*=15-23 for the respective strains. (C) Sperm number in WT, ΔFG and 2ΔFG young adult (YA) hermaphrodites. *n*=10-11 for the respective strains. (D) RBs were scored in respective genetic backgrounds with control and *byn-1* RNAi at 24 h in post-L4 stage hermaphrodites. *n*=31-40 for the respective conditions. (E) The number of sperm was quantified in respective genetic backgrounds with control and *byn-1* RNAi in YA hermaphrodites. *n*=11-19 for the respective conditions. (F) Confocal live images showing the localization of GLH-1::GFP and BYN-1::mCherry at the condensation zone in WT and 2ΔFG mutant males. Left: Male spermatogenesis at 20°C. Scale bar: 5 µm. Right: Enlarged diplotene and karyosome stages of spermatogenesis in WT and 2ΔFG mutants. Scale bar: 3 µm. (G) Colocalization of GLH-1::GFP and BYN-1::mCherry decreases in the condensation zone of 2ΔFG mutants. *n*=15 for each strain. (H) GLH-1::GFP-granule sizes at the condensation zone in the male germline quantified using ImageJ. *n*=40 for each strain. (I) Enlarged confocal live images of GLH-1::GFP and BYN-1::mCherry in the RBs of WT and 2ΔFG mutants. Scale bar: 3 µm. (J) Quantification of BYN-1::mCherry intensity in RBs of WT and 2ΔFG mutant males. *n*=9 for each strain. (K) Colocalization of GLH-1::GFP and BYN-1::mCherry in RBs of WT and 2ΔFG mutants. *n*=11 for each strain. Statistical significance for B-E calculated using one-way ANOVA, and for G,H,J,K a two-tailed, unpaired Student's *t*-test. ***P<0.001, *P<0.05. Error bars represent s.d.

important to look closer at the timing of these events, as the cytoplasmic colocalization of BYN-1 and GLH-1 initiates at the karyosome stage, and cell engulfment takes place moments later when spermatids bud. Determining whether engulfment can occur in the absence of budding will provide insight into the activation time and checkpoints of CED-1 pathways.

The results presented in this study point to BYN-1 acting upstream of CED-1 to promote programmed cell death. Interestingly, BYN-1/bystin is found in a rare syntenic group of tightly clustered orthologous genes present from single-cell eukaryotes to humans (Trachtulec and Forejt, 2001). The syntenic group includes programmed cell death 2 (PDCD2) and Unc93, an inducer of apoptosis, which might indicate a link between bystin and cell death programs. In hepatocellular carcinoma cells, BYSL is crucial for cell proliferation *in vitro* and *in vivo*; BYSL depletion increases apoptosis and suppresses nucleoli assembly after mitosis (Wang et al., 2009). Similarly, our study showed that *byn-1* RNAi also decreased germline stem cell proliferation, and increased physiological germ cell apoptosis in 48 h post L4-staged worms (Fig. S2B). It is unclear how the cytoplasmic interaction between BYN-1 and GLH-1 promotes RB internalization. In both trophoblasts and glioblastoma cells, cytoplasmic bystin promotes an epithelial-to-mesenchymal transition to mobilize cells (Sha et al., 2020; Sugihara et al., 2007). By extension, BYN-1 may help to mobilize or position RBs for uptake by the somatic gonad (Fig. 7B).

Conserved bystin/FG-repeat interactions signal cellular uptake

FG-repeat domains have been extensively studied within the context of the nuclear pore complex (NPC). In the NPC, unstructured FG-repeats extend into the central channel to establish a size-exclusion barrier between the nucleus and cytoplasm (Kim et al., 2018; Yamada et al., 2010). This size exclusion barrier is created by regularly spaced phenylalanines that interact to form a mesh or smart sieve (Schmidt and Görlich, 2015). Proteins smaller than 40 kDa diffuse through that sieve, whereas larger proteins and complexes must attach to a karyopherin to facilitate nucleocytoplasmic transport.

Development (2024) 151, dev202694. doi:10.1242/dev.202694

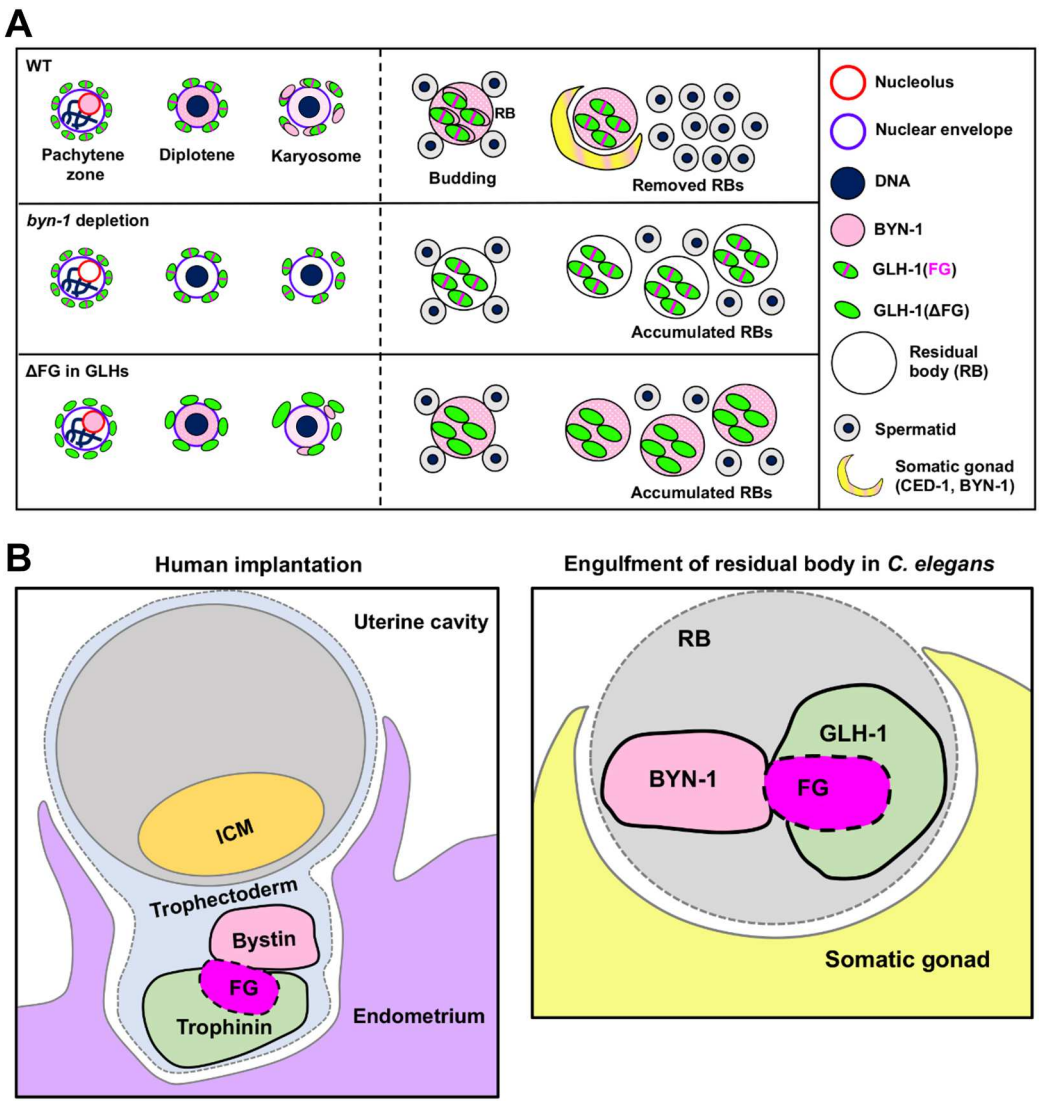

Fig. 7. Working model for BYN-1/bystin-mediated cellular engulfment. (A) The cytoplasmic translocation of BYN-1 appears to be required for activation of CED-1 for residual body (RB) engulfment during spermatogenesis. Upon nucleolar breakdown in the diplotene stage of spermatogenesis, BYN-1 disperses throughout the nucleoplasm. In the karyosome stage, BYN-1 leaves the nucleus where it colocalizes with GLH-1 in perinuclear germ granules. During the budding stage of spermatogenesis, GLH-1 and BYN-1 are deposited in anucleate RBs that become engulfed by CED-1-positive cells of the overlying somatic gonad. WT, wild type. (B) Similarities between human embryonic implantation and *C. elegans* RB clearance point to possible conservation of pathways that regulate cellular uptake. ICM, inner cell mass.

Of the 15 longest FG-repeat proteins in *C. elegans*, just six are components of the NPC (Shinkai et al., 2021). Another five (GLH-1, GLH-2, GLH-4, RDE-12 and DDX-19) are found in germ granules that cluster on the cytoplasmic surface of germ cell NPCs (Sheth et al., 2010), and another (PQN-75) is expressed in pharyngeal gland cells (Rochester et al., 2017). We previously showed that FG-repeat-rich germ granules extend the size exclusion barrier of NPCs further into the cytoplasm and, like FG-Nups, are disassembled with low concentrations of 1,6-hexanediol (Updike et al., 2011). GLH-containing granules can be detached from the periphery by removing their FG-repeat domains or by RNAi depletion of FG-Nup-encoding mRNAs (Marnik et al., 2019; Updike and Strome, 2009; Voronina and Seydoux, 2010).

In humans, seven of the 15 longest FG-repeat proteins are components of the NPC (Shinkai et al., 2021). Another seven are associated with keratin formation in the epidermis. The remaining protein is trophinin, which boasts the highest number of FG-repeats in the human proteome. Trophinin was initially shown to be, and primarily thought of as, an apical membrane protein in trophoblasts, but curiously it lacks the signal sequence for insertion into the plasma membrane. In fact, studies in which human trophoblastic teratocarcinoma HT-H cells were permeabilized to improve trophinin antibody accessibility, as well as COS-1 cells expressing recombinant trophinin, show the protein localizing to the cytoplasmic surface of the nuclear periphery (Aoyama et al., 2005). The distribution of cytoplasmic trophinin at the nuclear envelope is reminiscent of the perinuclear distribution of GLH proteins in *C. elegans* germ cells (Aoyama et al., 2005). By extension, trophinin may also be using its FG-repeats to extend the NPC size exclusion barrier into the cytoplasm of trophoblasts.

The cytoplasmic location of trophinin around the nuclear periphery could be where bystin first encounters its FG-repeats during embryonic implantation, mirroring the subcellular location where BYN-1 encounters GLH-1. Trophinin homologs are not found outside of placental mammals, and the protein itself could have resulted from a fusion between a MAGE domain and an FG-

Development (2024) 151, dev202694. doi:10.1242/dev.202694

repeat protein. Fusions of the FG-repeats of Nup98 are commonly found in acute myeloid leukemias and include fusions to DDX10, a DEAD-box helicase similar to GLH/DDX4 (Arai et al., 1997; Gough et al., 2011). However, the FG-repeats of trophinin are more similar to those of nematode GLH homologs than those of known mammalian FG-Nups (Fig. S1C). The affinity of BYN-1 for FG-repeat proteins may reflect an evolutionarily conserved function. However, considering the rapid evolution of sperm genes, the interaction between BYN-1 and GLH-1 could also represent a novel, sperm-specific role that evolved in *C. elegans*. In either scenario, *C. elegans* serves as a valuable model for deciphering the developmental, genetic and molecular events that occur when BYN-1/bystin encounters cytoplasmic FG-repeats. The dual-functional nature of BYN-1 appears to be determined and activated by subcellular localization, and *C. elegans* development provides a novel context for evaluating and discriminating these functions. Observations presented in this study suggest that efficient RB uptake and clearance may require BYN-1 in both the germline and soma, making it essential to determine whether BYN-1 binds other FG-repeat proteins in somatic cells where GLH proteins are not expressed. In doing so, the roles played by bystin, trophinin, and FG-repeat fusions in both embryonic implantation and cancer will become more apparent.

MATERIALS AND METHODS

C. elegans strains and maintenance

All strains of *C. elegans* were maintained and cultured on Nematode Growth Medium (NGM) agar plates at 20°C with standard protocols (Brenner, 1974). N2 (*C. elegans* wild isolate, Bristol variety) strain was used as wild-type control for this study. The following strains were created for this study:
DUP261: *glh-1(sam24[glh-1::gfp::3xFlag])* I; *byn-1(sam159[byn-1::mCherry::V5])* III.
DUP263: *glh-2(sam83[ΔFGglh-2]) glh-1(sam72[ΔFGglh-1::gfp::3xFlag])* I; *byn-1[sam159(byn-1::mCherry::V5)]* III.
DUP313: *byn-1[sam159(byn-1::mCherry::V5)]* III.
DUP315: *glh-1(sam24[glh-1::gfp::3xFlag])/hT2g [bli-4(e937) let-?(q782) qIs48]* I; *byn-1*sam188([Δbyn-1::mCherry::V5])/hT2 [bli-4(e937) let-?(q782) qIs48]* III.

GenBank-formatted sequence files for the two CRISPR-generated *byn-1* alleles, *sam159* and *sam188*, are available on Figshare (https://doi.org/10.6084/m9.figshare.26132659.v1).

Strains that have been described previously (Marnik et al., 2019) were:
DUP64: *glh-1(sam24[glh-1::gfp::3xFlag])* I.
DUP163: *glh-1(sam72[ΔFGglh-1::gfp::3xFlag])* I; *itIs37[pie-1p::mCherry::H2B::pie-1 3′UTR, unc-119(+)]* IV.
DUP165: *glh-2(sam83[ΔFGglh-2]) glh-1(sam72[ΔFGglh-1::gfp::3xFlag])* I; *itIs37[pie-1p::mCherry::H2B::pie-1 3′UTR, unc-119(+)]* IV.
DUP143: *glh-1(sam64[T663Aglh-1::gfp::3xFlag])* I.
SS940: *bnIs1(pie-1p::GFP::PGL-1)* I; *fog-2(q71)* V.
DUP151: *glh-1(sam71[ΔZFglh-1::gfp::3xFlag])* I.
DUP170: *glh-2(sam89[DEADtoDAADglh-2) glh-1(sam90[DEADtoDAADglh-1::gfp::3xFlag]) I/hT2[bli-4(e937) let-?(q782) qIs48]* (I;III).

Strains obtained from the CGC were:
DCL569: *mkcSi13 [sun-1p::rde-1::sun-1 3′UTR+unc-119(+)]* II; *rde-1(mkc36)* V.
NL3511: *ppw-1(pk1425)* I.
NL2099: *rrf-3(pk1426)* II.
CU1546: *smIs34[ced-1p::ced-1::GFP+rol-6(su1006)]*.
CB3203: *ced-1(e1735)* I.
MT11068: *ced-12(n3261)* I.

CRISPR/Cas9 gene editing

CRISPR/Cas9 editing was performed as described by Ghanta and Mello (2020). *byn-1[sam159(byn-1::mCherry::V5]* was created using the 20 bp crRNA AGGCCGAAAGACGGATAGTA and a homologous repair (HR) template to insert mCherry::V5 in-frame before the stop codon. *byn-1[sam188(Δbyn-1::mCherry::V5)]* was created using a left-flanking crRNA ATTCCTTTTCACCATGTTAC, a right-flanking crRNA ATAAATAG-CTGCCTTCTGCT, and an HR template GTAATTCTGCTAATTTTTA-ATTATGAATTTCCAGTAGGCAGCTATTTATGAGCTGATCAGAGTA-AGTT to create a 1608 bp deletion in the *byn-1[sam159(byn-1::mCherry::V5]* background, starting 2 bp upstream of the ATG start codon through most of the ninth exon, also turning off any *mCherry* expression. This deletion does not disrupt F57B9.8, which is encoded on the opposite strand of the last intron of *byn-1* (Fig. S3A).

Yeast two-hybrid screen

ULTImate Y2H™ screening was performed by Hybrigenics Services, S.A.S., Evry, France (http://www.hybrigenics-services.com). The coding sequence for full-length *C. elegans glh-1* (NM_059562.6) was PCR-amplified and cloned into pB29 as an N-terminal fusion to LexA (glh-1-LexA). The construct was checked by sequencing the entire insert and used as a bait to screen a random-primed *C. elegans* mixed-stages cDNA library constructed into pP6. pB29 and pP6 derive from the original pBTM116 and pGADGH plasmids, respectively (Béranger et al., 1997; Vojtek and Hollenberg, 1995). Eighty million clones (eightfold the complexity of the library) were screened using a mating approach with YHGX13 (Y187 ade2-101::loxP-kanMX-loxP, matα) and L40ΔGal4 (mata) yeast strains as previously described (Fromont-Racine et al., 1997) and 232 His^+ colonies were selected on a medium lacking tryptophan, leucine and histidine. The prey fragments of the positive clones were amplified by PCR and sequenced at their 5′ and 3′ junctions. The resulting sequences were used to identify the corresponding interacting proteins in the GenBank database (NCBI) using a fully automated procedure. A confidence score (PBS, for Predicted Biological Score) was attributed to each interaction as previously described (Formstecher et al., 2005). The PBS relies on two different levels of analysis. First, a local score takes into account the redundancy and independency of prey fragments, as well as the distribution of reading frames and stop codons in overlapping fragments. Second, a global score takes into account the interactions found in all the screens performed at Hybrigenics using the same library. This global score represents the probability of an interaction being nonspecific. For practical use, the scores were divided into four categories, from ‘A’ (highest confidence) to ‘D’ (lowest confidence). A fifth category (‘E’) specifically flags interactions involving highly connected prey domains previously found several times in screens performed on libraries derived from the same organism. Finally, several of these highly connected domains have been confirmed as false positives of the technique and are now tagged as ‘F’. The PBS scores have been shown to positively correlate with the biological significance of interactions (Rain et al., 2001; Wojcik et al., 2002). Of the 232 processed clones, 117 received high (‘B’) or very high (‘A’) PBS scores in fragments encoded by six different genes (Table S1). Six of the 117 corresponded to a C-terminal fragment (aa 377-449) of BYN-1.

1×1 Y2H assay

The coding sequences for the fragments containing amino acids 1-152 and 153-763 of *C. elegans glh-1* (NM_059562.6) were PCR-amplified and cloned into pB29 as N-terminal fusion to LexA (*glh-1*-fragments-LexA). The constructs were checked by sequencing the entire inserts. The fragment corresponding to amino acids 372-449 of *byn-1* was extracted from the ULTImate Y2H™ screening of full-length *glh-1* with the *C. elegans* mixed-stages library. It was cloned in-frame with the Gal4 activation domain (AD) into plasmid pP6. The AD construct was checked by sequencing. Bait and prey constructs were transformed in the yeast haploid cells L40ΔGal4 (mata) and YHGX13 (Y187 ade2-101::loxP-kanMX-loxP, matα), respectively. The diploid yeast cells were obtained using a mating protocol with both yeast strains (Fromont-Racine et al., 1997). These assays are based on the HIS3 reporter gene (growth assay without histidine). As negative controls, the bait plasmids were tested in the presence of empty prey vector (pP6) and the prey plasmid was tested with an empty bait vector that allows the expression of LexA (pB27). The interaction between SMAD and SMURF was used as positive control (Colland et al., 2004). Controls and interactions were first tested in the form of streaks of three independent yeast clones on DO-2 and DO-3 selective media. The DO-2 selective medium lacking tryptophan and leucine was used as a growth control and to verify the

Development (2024) 151, dev202694. doi:10.1242/dev.202694

presence of the bait and prey plasmids. The DO-3 selective medium without tryptophan, leucine and histidine selects for the interaction between bait and prey. Interaction pairs were then tested in duplicate in the form of calibrated drops as two independent clones were picked for the growth assay. For each interaction, several dilutions (undiluted, 10^{-1}, 10^{-2}, 10^{-3}) of the diploid yeast cells (culture normalized at 5×10^{7} cells) and expressing both bait and prey constructs were spotted on several selective media. The DO-2 selective medium lacking tryptophan and leucine was used as a growth control and to verify the presence of both the bait and prey plasmids. The different dilutions were also spotted on a selective medium without tryptophan, leucine and histidine (DO-3). Four different concentrations of 3-aminotriazole (1, 5, 10 and 50 mM), an inhibitor of the HIS3 gene product, were added to the DO-3 plates to increase stringency.

RNAi knockdown

Depletion of *byn-1* was performed using the bacteria-mediated (feeding) method as described previously (Kamath et al., 2003). *Escherichia coli* strain HT115(DE3) containing F57B9.5 (*byn-1*) inserted L4440 vector was obtained from the Vidal library (Rual et al., 2004). Sequencing of this first *byn-1* RNAi clone revealed it contains a 139 bp insertion targeting part of exon 9 and all of exon 10. The second RNAi clone, pDU103, was generated by inserting 270 bp of the *byn-1* mRNA sequence (overlapping the first two exons) into HindIII sites of the L4440 plasmid, which was then re-transformed into HT115(DE). L4440 in HT115(DE3) was used as the RNAi control. Synchronized L1 or L4 larval-stage worms were placed on feeding RNAi plates and were incubated at 20°C for phenotypic analysis.

byn-1 qRT-PCR

Three-hundred adult hermaphrodites were collected in TRIzol (Invitrogen) for each condition, and total RNA was extracted using a phase lock gel (MaXtract High Density, QIAGEN). cDNA was synthesized using oligo-dT primer and M-MLV reverse transcriptase (Invitrogen). qRT-PCR assays were performed using SYBR Green PCR Master Mix (Applied Biosystems). The final PCR volume was 10 µl. *act-1* mRNA was used as an endogenous control for data normalization. The primers used for the measurement of expression of the *byn-1* gene were as follows: *byn-1* forward, 5′-AAGATGCTATCCAAATGTCCAC-3′; *byn-1* reverse, 5′-GTCACGCATATTAAACTCATTCGG-3′; *act-1* forward, 5′-CCAGGAATTGCTGATCGTATGCAGAA-3′; *act-1* reverse, 5′-TGGAGAGGGAAGCGAGGATAG-3′.

Analysis of brood size, embryonic lethality, eggshell integrity, and developmental growth

Synchronized L4-stage hermaphrodites were moved to individual plates seeded with control RNAi or *byn-1* RNAi bacteria and allowed to lay eggs for 24 h at 20°C. Each worm was transferred to a new plate every 24 h for 4 days. The number of progeny was calculated as the total number of non-hatched and hatched embryos produced by a single mother. Embryonic lethality was calculated as the percentage of non-hatched embryos out of the total number of embryos produced for 4 days. To investigate eggshell integrity, membrane permeability was assessed using FM1-43 dye (Sigma-Aldrich), as previously described (Nakayama et al., 2009). In brief, either control or *byn-1* RNAi-treated mothers were dissected in 150 mM KCl with 30 mM of FM1-43 dye to observe embryos. The proportion of embryos infiltrated by FM1-43 was measured using a Leica Thunder Imager Live Cell microscope with an HC PL APO 40×/0.95 DRY objective. For each case, three independent experiments were performed. Percentage larval development was calculated as the percentage of larvae out of the total number of hatched embryos that reached each developmental stage, as previously described (Min et al., 2015).

Fluorescence microscopy and image analysis

Fluorescence microscopy and image processing were performed as previously described (Rochester et al., 2022; Spaulding et al., 2022). In brief, GFP- and mCherry-tagged fluorescent proteins were visualized in living worms or dissected embryos by mounting on 2% agarose pads with M9 buffer with 10 mM levamisole. Live fluorescent images were captured using a point scanning confocal unit (LSM980, Carl Zeiss Microscopy) on a Zeiss Axio Examiner Z1 upright microscope stand equipped with a Zeiss Plan Apo 63×/1.4 NA Oil (420782-9900-799) objective and Immersol 518F Immersion Oil. sGFP and mCherry fluorescence were excited with the 488 nm diode (0.2% laser power) and the 561 nm DPSS laser (2% power), and collected using Airyscan2 with the following detection wavelengths: sGFP (499-548 nm) and mCherry (574-627 nm). Images were sequentially acquired in Super Resolution mode (SR) at zoom 10, with a line average of 1, a resolution of 292×292 pixels, 0.043×0.043 µm pixel size, a pixel time of 0.69 µs, in 16-bit, and in bidirectional mode. *z*-stack images were collected with a step size of 0.150 µm, 3.3 µm deep, with the Motorized Scanning Stage 130×85 PIEZO (Carl Zeiss Microscopy) mounted on Z-piezo stage insert WSB500. Airyscan images were processed using the 'auto' mode in Zen Blue Software (Zen Pro 3.1) and saved in CZI format. Live image processing and quantification of fluorescent proteins were performed using Fiji and ImageJ. Single-slice images of gonads and images from maximum intensity projections of *z*-series of gonads were used for quantification. Image thresholds were set manually, regions of interest were selected, and areas of regions of interest were measured. To quantify the colocalization of GLH-1 and BYN-1 during sperm differentiation, we used ImageJ with the plugin JACoP to calculate Pearson's colocalization coefficient. To analyze the intensity of BYN-1 in RBs, the measure tool was applied to measure integrated density. Mean pixel intensity was subtracted from the background to calculate the corrected total cell fluorescence [CTCF=integrated density – (area of cell×mean background fluorescence)] using ImageJ. Fixed immunofluorescent images and FM1-43 staining were observed on a Leica Thunder Imager Live Cell microscope with an HC PL APO 63×/1.47 Oil CORR TIRF objective and DAPI, GFP and TXR filter sets. Images were acquired with a Leica DFC9000 CT deep-cooled sCMOS camera and Leica LAS X imaging software. To observe the progression of spermatogenesis in males, worms were dissected and fixed with 100% methanol at −20°C for 10 min, followed by 100% acetone fixation at −20°C for 10 min. The specimens were further counterstained with DAPI to stain DNA. The following primary and secondary antibodies were used in this study: mouse monoclonal anti-a-tubulin (1:500; Sigma-Aldrich, T9026), rabbit anti-phospho-histone H3 (Ser10) (1:500; EMD Millipore, 06-570), Alexa Fluor 488-conjugated goat anti-mouse IgG (1:500; Invitrogen, A32723), Alexa Fluor 594-conjugated goat anti-rabbit IgG (1:500; Invitrogen, A32740).

Annexin V staining and quantification of RBs

Annexin V staining and quantification of RBs were performed as previously described with some modifications (Huang et al., 2012). In brief, single males were placed in 3×3 drops (15 µl) of sperm medium (SM) buffer (50 mM HEPES, 25 mM KCl, 45 mM $MgSO_4$, 5 mM $CaCl_2$ and 10 mM dextrose, pH 7.8) on GCP-coated slides [0.2% gelatin (USP), 0.002% chrome alum (Sigma-Aldrich), 1 mg/ml poly-L-lysine (Sigma-Aldrich)]. Males were dissected in a drop of SM buffer containing 0.5 µl Alexa Fluor 488-conjugated Annexin V (Molecular Probes) on a GCP slide to release RBs and sperm and incubated in a wet chamber for 20 min at room temperature. A coverslip was gently overlaid and sealed with Vaseline. The samples were observed under Nomarski differential interference contrast (DIC) microscopy, and RBs with Annexin V were counted using a Leica DFC9000 GT microscope. In hermaphrodites, RBs were counted in the proximal gonad arm at two different time points (6 h and 24 h post-L4 stage) using Nomarski optics.

Spermatid quantification assay

Spermatid quantification assay was performed as previously described with minor modifications (Huang et al., 2012). Briefly, a single hermaphrodite or a single male (5 h post-L4 stage) was picked into a small drop of fixation buffer on a slide and the gonad dissected to release sperm. The sample was then fixed with 4% paraformaldehyde for 20 min at room temperature, washed three times with PBST (1.4 M NaCl, 0.03 M KCl, 0.1 M Na_2HPO_4, 0.02 M KH_2PO_4, 0.2% Tween 20, pH 7.2), and further fixed with 70% ethanol at 4°C overnight. Then, the sample was washed twice with PBST and stained with DAPI. Sperm nuclei were counted in each gonad arm, and at least ten worms were scored for each genotype.

Fertility assay by mating

Synchronized adult males were mated with *fog-2* females in a 3:1 ratio for 6 h. Mated *fog-2* females were subsequently transferred to new NGM plates, and the fertilized eggs in the uterus were quantified.

Development (2024) 151, dev202694. doi:10.1242/dev.202694

GLH-1 co-immunoprecipitation

Anti-FLAG-M2 magnetic beads (Sigma-Aldrich, M8823) were resuspended by gentle inversion, washed in cold TBS three times and left in TBS on ice during the following sample preparation. Approximately 400-500 µl of synchronized young adult DUP64, DUP261 and DUP313 worms were washed off plates with dH_2O and flash-frozen in liquid nitrogen. Frozen worm pellets were ground into a fine powder using a mortar and pestle in liquid nitrogen. The powder was resuspended in 1 ml of lysis buffer [25 mM HEPES-KOH, pH 7.4, 10 mM potassium acetate (KOAc), 2 mM $Mg(OAc)_2$, 100 mM KCl, 0.25% Triton X-100, 1 mM PMSF, one cOmplete protease inhibitor tablet]. Samples were spun at 12,000 ***g*** for 5 min at 4°C then 1 ml of supernatant was added to 100 µl of beads and rotated at 4°C overnight. Beads were washed three times with 1 ml of cold TBS. Protein was eluted by incubating beads in 250 µl of 0.1 M glycine HCl, pH 3.0, at room temperature for 5 min with gentle shaking. Eluate was transferred to fresh tubes containing 10 µl of 0.5 M Tris-HCl, pH 7.4, with 1.5 M NaCl. Elution was repeated and the second eluate was added to the same tube (total eluate is 500 µl). Eluate was added 1:1 to 2× Laemmli buffer (10% BME, 4% SDS, 20% glycerol, 0.004% Bromophenol Blue, 0.125 M Tris-Cl pH 6.8) and boiled for 5 min. Then, 40 µl of sample was loaded onto a mini-PROTEAN TGX stain-free gel (Bio-Rad, 4568084) and run at 200 V for 25 min in SDS running buffer (0.2501 M Tris base, 1.924 M glycine, 0.0347 M SDS). The contents of the gel were transferred using a trans-blot turbo transfer pack (Bio-Rad, 1704156) on the Bio-Rad Trans-Blot Turbo Transfer System. The PVDF membrane was blocked in 5% nonfat milk in TBST (20 mM Tris-HCl pH 7.4, 150 mM NaCl, 0.1% Tween 20) at room temperature for 1 h. The membrane was incubated overnight at 4°C with mouse monoclonal anti-V5 (Thermo Fisher Scientific, R960; 1:5000) and mouse monoclonal anti-FLAG M2 (Sigma-Aldrich, F1804; 1:5000) in 5% milk and then washed six times, 10 min each wash, in TBST at room temperature. The membrane was then incubated in goat anti-mouse IgG-HRP (Invitrogen, 31430; 1:10,000) in 5% milk for 1 h at room temperature and washed six times, 10 min each wash, in TBST. Finally, the membrane was developed using Clarity Western ECL Substrate (Bio-Rad, 1705060S) and imaged on a Syngene G:Box gel and blot imaging system.

Germ cell proliferation assay

To observe the mitotic germ cells at the distal region of gonad, worms were dissected and fixed with 100% methanol at −20°C for 10 min, followed by 100% acetone fixation at −20°C for 10 min. The specimens were immunostained using rabbit anti-phospho-histone H3 (Ser10) (1:500; EMD Millipore, 06-570) and Alexa Fluor 594-conjugated goat anti-rabbit IgG (1:500; Invitrogen, A32740).

Germline apoptosis assay

Germ cell corpses were counted under Nomarski DIC microscopy at 24 h and 48 h post-L4 stages of hermaphrodites as previously described (Gumienny et al., 1999). Apoptotic germ cells were visualized by Acridine Orange vital staining as previously described (Navarro et al., 2001). Briefly, 24 h and 48 h post-L4 stage worms were stained with 25 µg/ml Acridine Orange in M9 buffer for 1 h in the dark, allowed to recover on new NGM plates for 30 min and observed under fluorescence microscopy to count the number of Acridine Orange-positive germ cells per gonad arm. Only one gonad arm was scored for each observed animal, and 15-20 animals were examined for each condition.

Phalloidin staining

Phalloidin staining was performed as described previously with modifications (Huang et al., 2012). Males were fixed with 4% paraformaldehyde at room temperature for 20 min and further fixed with 70% ethanol. The samples were rinsed three times for 10 min each in PBST. The samples were incubated with rhodamine-conjugated phalloidin (Molecular Probes, Life Technologies) for 2 h, and then washed with PBST for 10 min. Fixed fluorescent images were observed on a Leica Thunder Imager microscope with an HC PL APO 63×/1.47 Oil CORR TIRF objective. Images were acquired with a Leica DFC9000 CT deep-cooled sCMOS camera and Leica LAS X imaging software.

Statistical analysis

Statistical analysis was performed using GraphPad Prism 9.3.1 software. *P*-values lower than 0.05 were considered statistically significant. Data graphs were plotted in GraphPad Prism as scatter dot plots with error bar or bar graphs displaying mean±s.d. *P*-values are represented by asterisks and *n* values for each experiment are denoted in the corresponding figure panel, figure legend or bar graph.

Acknowledgements

We acknowledge support from Chris Smith in the MDI Biological Laboratory (MDIBL) Sequencing Facility for Sanger sequencing services; Frederic Bonnet in the MDIBL Light Microscopy Facility for training, assistance and use of super-resolution image acquisition; and plate pouring services provided by the MDIBL Animal Resources Core. MDIBL Cores and Facilities receive support from the National Institutes of Health [Maine INBRE GM103423, MDIBL COBRE GM104318]. Some of the strains for this study were provided by the CGC, funded by National Institutes of Health Office of Research Infrastructure Programs OD010440.

Competing interests

The authors declare no competing or financial interests.

Author contributions

Conceptualization: H.M., D.L.U.; Methodology: H.M.; Validation: H.M.; Formal analysis: H.M.; Investigation: H.M., E.L.S., C.S.S., P.G., N.L., D.L.U.; Resources: C.S.S., E.J., L.S.M.P., D.L.U.; Data curation: H.M.; Writing - original draft: H.M., D.L.U.; Writing - review & editing: H.M., D.L.U.; Visualization: H.M., E.L.S.; Supervision: D.L.U.; Project administration: D.L.U.; Funding acquisition: H.M., D.L.U.

Funding

This work was funded by the Basic Science Research Program of the National Research Foundation of Korea [RS-2023-00246465 to H.M.], the National Science Foundation REU program [DBI-2243416 to E.J. and L.M.P.], a National Research Service Award from the National Institutes of Health [GM143851 to E.L.S.], and the National Institute of General Medical Sciences [GM152109 to D.L.U.]. Deposited in PMC for release after 12 months.

Data availability

GenBank-formatted sequence files for the two CRISPR-generated *byn-1* alleles, *sam159* and *sam188*, are available on Figshare (https://doi.org/10.6084/m9.figshare.26132659.v1).

References

Adachi, K., Soeta-Saneyoshi, C., Sagara, H. and Iwakura, Y. (2007). Crucial role of Bysl in mammalian preimplantation development as an integral factor for 40S ribosome biogenesis. *Mol. Cell. Biol.* **27**, 2202-2214. doi:10.1128/MCB.01908-06

Aoki, R., Suzuki, N., Paria, B. C., Sugihara, K., Akama, T. O., Raab, G., Miyoshi, M., Nadano, D. and Fukuda, M. N. (2006). The Bysl gene product, bystin, is essential for survival of mouse embryos. *FEBS Lett.* **580**, 6062-6068. doi:10.1016/j.febslet.2006.09.072

Aoyama, J., Nakayama, Y., Sugiyama, D., Saburi, S., Nadano, D., Fukuda, M. N. and Yamaguchi, N. (2005). Apical cell adhesion molecule, trophinin, localizes to the nuclear envelope. *FEBS Lett.* **579**, 6326-6332. doi:10.1016/j.febslet.2005.10.012

Arai, Y., Hosoda, F., Kobayashi, H., Arai, K., Hayashi, Y., Kamada, N., Kaneko, Y. and Ohki, M. (1997). The inv(11)(p15q22) chromosome translocation of de novo and therapy-related myeloid malignancies results in fusion of the nucleoporin gene, NUP98, with the putative RNA helicase gene, DDX10. *Blood* **89**, 3936-3944. doi:10.1182/blood.V89.11.3936

Ayala, G. E., Dai, H., Li, R., Ittmann, M., Thompson, T. C., Rowley, D. and Wheeler, T. M. (2006). Bystin in perineural invasion of prostate cancer. *Prostate* **66**, 266-272. doi:10.1002/pros.20323

Béranger, F., Aresta, S., de Gunzburg, J. and Camonis, J. (1997). Getting more from the two-hybrid system: N-terminal fusions to LexA are efficient and sensitive baits for two-hybrid studies. *Nucleic Acids Res.* **25**, 2035-2036. doi:10.1093/nar/25.10.2035

Brenner, S. (1974). The genetics of Caenorhabditis elegans. *Genetics* **77**, 71-94. doi:10.1093/genetics/77.1.71

Chen, W., Hu, Y., Lang, C. F., Brown, J. S., Schwabach, S., Song, X., Zhang, Y., Munro, E., Bennett, K., Zhang, D. et al. (2020). The dynamics of P granule liquid droplets are regulated by the Caenorhabditis elegans germline RNA helicase GLH-1 via its ATP hydrolysis cycle. *Genetics* **215**, 421-434. doi:10.1534/genetics.120.303052

Colland, F., Jacq, X., Trouplin, V., Mougin, C., Groizeleau, C., Hamburger, A., Meil, A., Wojcik, J., Legrain, P. and Gauthier, J.-M. (2004). Functional proteomics mapping of a human signaling pathway. *Genome Res.* **14**, 1324-1332. doi:10.1101/gr.2334104

Curran, S. P. and Ruvkun, G. (2007). Lifespan regulation by evolutionarily conserved genes essential for viability. *PLoS Genet.* **3**, e56. doi:10.1371/journal.pgen.0030056

Dalton, H. M. and Curran, S. P. (2018). Hypodermal responses to protein synthesis inhibition induce systemic developmental arrest and AMPK-dependent survival in Caenorhabditis elegans. *PLoS Genet.* **14**, e1007520. doi:10.1371/journal.pgen.1007520

Formstecher, E., Aresta, S., Collura, V., Hamburger, A., Meil, A., Trehin, A., Reverdy, C., Betin, V., Maire, S., Brun, C. et al. (2005). Protein interaction mapping: a Drosophila case study. *Genome Res.* **15**, 376-384. doi:10.1101/gr.2659105

Fromont-Racine, M., Rain, J. C. and Legrain, P. (1997). Toward a functional analysis of the yeast genome through exhaustive two-hybrid screens. *Nat. Genet.* **16**, 277-282. doi:10.1038/ng0797-277

Fukuda, M. N. and Nozawa, S. (1999). Trophinin, tastin, and bystin: a complex mediating unique attachment between trophoblastic and endometrial epithelial cells at their respective apical cell membranes. *Semin Reprod Endocrinol* **17**, 229-234. doi:10.1055/s-2007-1016230

Fukuda, M. N. and Sugihara, K. (2008). An integrated view of L-selectin and trophinin function in human embryo implantation. *J. Obstet. Gynaecol. Res.* **34**, 129-136. doi:10.1111/j.1447-0756.2008.00776.x

Fukuda, M. N., Miyoshi, M. and Nadano, D. (2008). The role of bystin in embryo implantation and in ribosomal biogenesis. *Cell. Mol. Life Sci.* **65**, 92-99. doi:10.1007/s00018-007-7302-9

Ghanta, K. S. and Mello, C. C. (2020). Melting dsDNA donor molecules greatly improves precision genome editing in caenorhabditis elegans. *Genetics* **216**, 643-650. doi:10.1534/genetics.120.303564

Gough, S. M., Slape, C. I. and Aplan, P. D. (2011). NUP98 gene fusions and hematopoietic malignancies: common themes and new biologic insights. *Blood* **118**, 6247-6257. doi:10.1182/blood-2011-07-328880

Green, R. A., Kao, H.-L., Audhya, A., Arur, S., Mayers, J. R., Fridolfsson, H. N., Schulman, M., Schloissnig, S., Niessen, S., Laband, K. et al. (2011). A high-resolution C. elegans essential gene network based on phenotypic profiling of a complex tissue. *Cell* **145**, 470-482. doi:10.1016/j.cell.2011.03.037

Green, R. A., Khaliullin, R. N., Zhao, Z., Ochoa, S. D., Hendel, J. M., Chow, T.-L., Moon, H., Biggs, R. J., Desai, A. and Oegema, K. (2024). Automated profiling of gene function during embryonic development. *Cell* **187**, 3141-3160.e23. doi:10.1016/j.cell.2024.04.012

Gumienny, T. L., Lambie, E., Hartwieg, E., Horvitz, H. R. and Hengartner, M. O. (1999). Genetic control of programmed cell death in the Caenorhabditis elegans hermaphrodite germline. *Development* **126**, 1011-1022. doi:10.1242/dev.126.5.1011

Hamatani, T., Daikoku, T., Wang, H., Matsumoto, H., Carter, M. G., Ko, M. S. H. and Dey, S. K. (2004). Global gene expression analysis identifies molecular pathways distinguishing blastocyst dormancy and activation. *Proc. Natl. Acad. Sci. USA* **101**, 10326-10331. doi:10.1073/pnas.0402597101

Hansen, M., Taubert, S., Crawford, D., Libina, N., Lee, S. J. and Kenyon, C. (2007). Lifespan extension by conditions that inhibit translation in Caenorhabditis elegans. *Aging Cell* **6**, 95-110. doi:10.1111/j.1474-9726.2006.00267.x

Huang, J., Wang, H., Chen, Y., Wang, X. and Zhang, H. (2012). Residual body removal during spermatogenesis in C. elegans requires genes that mediate cell corpse clearance. *Development* **139**, 4613-4622. doi:10.1242/dev.086769

Kamath, R. S., Fraser, A. G., Dong, Y., Poulin, G., Durbin, R., Gotta, M., Kanapin, A., Le Bot, N., Moreno, S., Sohrmann, M. et al. (2003). Systematic functional analysis of the Caenorhabditis elegans genome using RNAi. *Nature* **421**, 231-237. doi:10.1038/nature01278

Kim, S. J., Fernandez-Martinez, J., Nudelman, I., Shi, Y., Zhang, W., Raveh, B., Herricks, T., Slaughter, B. D., Hogan, J. A., Upla, P. et al. (2018). Integrative structure and functional anatomy of a nuclear pore complex. *Nature* **555**, 475-482. doi:10.1038/nature26003

Marnik, E. A., Fuqua, J. H., Sharp, C. S., Rochester, J. D., Xu, E. L., Holbrook, S. E. and Updike, D. L. (2019). Germline maintenance through the multifaceted activities of GLH/Vasa in Caenorhabditis elegans P granules. *Genetics* **213**, 923-939. doi:10.1534/genetics.119.302670

Min, H., Kawasaki, I., Gong, J. and Shim, Y.-H. (2015). Caffeine induces high expression of cyp-35A family genes and inhibits the early larval development in Caenorhabditis elegans. *Mol. Cells* **38**, 236-242. doi:10.14348/molcells.2015.2282

Miyoshi, M., Okajima, T., Matsuda, T., Fukuda, M. N. and Nadano, D. (2007). Bystin in human cancer cells: intracellular localization and function in ribosome biogenesis. *Biochem. J.* **404**, 373-381. doi:10.1042/BJ20061597

Nakayama, J., Aoki, D., Suga, T., Akama, T. O., Ishizone, S., Yamaguchi, H., Imakawa, K., Nadano, D., Fazleabas, A. T., Katsuyama, T. et al. (2003). Implantation-dependent expression of trophinin by maternal fallopian tube epithelia during tubal pregnancies: possible role of human chorionic gonadotrophin on ectopic pregnancy. *Am. J. Pathol.* **163**, 2211-2219. doi:10.1016/S0002-9440(10)63579-1

Nakayama, Y., Shivas, J. M., Poole, D. S., Squirrell, J. M., Kulkoski, J. M., Schleede, J. B. and Skop, A. R. (2009). Dynamin participates in the maintenance of anterior polarity in the Caenorhabditis elegans embryo. *Dev. Cell* **16**, 889-900. doi:10.1016/j.devcel.2009.04.009

Navarro, R. E., Shim, E. Y., Kohara, Y., Singson, A. and Blackwell, T. K. (2001). cgh-1, a conserved predicted RNA helicase required for gametogenesis and protection from physiological germline apoptosis in C. elegans. *Development* **128**, 3221-3232. doi:10.1242/dev.128.17.3221

Pan, K. Z., Palter, J. E., Rogers, A. N., Olsen, A., Chen, D., Lithgow, G. J. and Kapahi, P. (2007). Inhibition of mRNA translation extends lifespan in Caenorhabditis elegans. *Aging Cell* **6**, 111-119. doi:10.1111/j.1474-9726.2006.00266.x

Price, I. F., Hertz, H. L., Pastore, B., Wagner, J. and Tang, W. (2021). Proximity labeling identifies LOTUS domain proteins that promote the formation of perinuclear germ granules in C. elegans. *eLife* **10**, e72276. doi:10.7554/eLife.72276

Rain, J. C., Selig, L., De Reuse, H., Battaglia, V., Reverdy, C., Simon, S., Lenzen, G., Petel, F., Wojcik, J., Schächter, V. et al. (2001). The protein-protein interaction map of Helicobacter pylori. *Nature* **409**, 211-215. doi:10.1038/35051615

Rochester, J. D., Tanner, P. C., Sharp, C. S., Andralojc, K. M. and Updike, D. L. (2017). PQN-75 is expressed in the pharyngeal gland cells of Caenorhabditis elegans and is dispensable for germline development. *Biol. Open* **6**, 1355-1363. doi:10.1242/bio.027987

Rochester, J. D., Min, H., Gajjar, G. A., Sharp, C. S., Maki, N. J., Rollins, J. A., Keiper, B. D., Graber, J. H. and Updike, D. L. (2022). GLH-1/Vasa represses neuropeptide expression and drives spermiogenesis in the C. elegans germline. *Dev. Biol.* **492**, 200-211. doi:10.1016/j.ydbio.2022.10.003

Roos, J., Luz, J. M., Centoducati, S., Sternglanz, R. and Lennarz, W. J. (1997). ENP1, an essential gene encoding a nuclear protein that is highly conserved from yeast to humans. *Gene* **185**, 137-146. doi:10.1016/S0378-1119(96)00661-0

Rual, J.-F., Ceron, J., Koreth, J., Hao, T., Nicot, A.-S., Hirozane-Kishikawa, T., Vandenhaute, J., Orkin, S. H., Hill, D. E., van den Heuvel, S. et al. (2004). Toward improving Caenorhabditis elegans phenome mapping with an ORFeome-based RNAi library. *Genome Res.* **14**, 2162-2168. doi:10.1101/gr.2505604

Saijou, E., Fujiwara, T., Suzaki, T., Inoue, K. and Sakamoto, H. (2004). RBD-1, a nucleolar RNA-binding protein, is essential for Caenorhabditis elegans early development through 18S ribosomal RNA processing. *Nucleic Acids Res.* **32**, 1028-1036. doi:10.1093/nar/gkh264

Schmidt, H. B. and Görlich, D. (2015). Nup98 FG domains from diverse species spontaneously phase-separate into particles with nuclear pore-like permselectivity. *eLife* **4**, 1-30. doi:10.7554/eLife.04251

Sengoku, T., Nureki, O., Nakamura, A., Kobayashi, S. and Yokoyama, S. (2006). Structural basis for RNA unwinding by the DEAD-box protein drosophila vasa. *Cell* **125**, 287-300. doi:10.1016/j.cell.2006.01.054

Sha, Z., Zhou, J., Wu, Y., Zhang, T., Li, C., Meng, Q., Musunuru, P. P., You, F., Wu, Y., Yu, R. et al. (2020). BYSL Promotes glioblastoma cell migration, invasion, and mesenchymal transition through the GSK-3β/β-catenin signaling pathway. *Front Oncol* **10**, 565225. doi:10.3389/fonc.2020.565225

Shakes, D. C., Wu, J.-C., Sadler, P. L., Laprade, K., Moore, L. L., Noritake, A. and Chu, D. S. (2009). Spermatogenesis-specific features of the meiotic program in Caenorhabditis elegans. *PLoS Genet.* **5**, e1000611. doi:10.1371/journal.pgen.1000611

Sheth, U., Pitt, J., Dennis, S. and Priess, J. R. (2010). Perinuclear P granules are the principal sites of mRNA export in adult C. elegans germ cells. *Development* **137**, 1305-1314. doi:10.1242/dev.044255

Shinkai, Y., Kuramochi, M. and Miyafusa, T. (2021). New family members of FG repeat proteins and their unexplored roles during phase separation. *Front. Cell Dev. Biol.* **9**, 708702. doi:10.3389/fcell.2021.708702

Smith, P., Leung-Chiu, W.-M., Montgomery, R., Orsborn, A., Kuznicki, K., Gressman-Coberly, E., Mutapcic, L. and Bennett, K. (2002). The GLH proteins, Caenorhabditis elegans P granule components, associate with CSN-5 and KGB-1, proteins necessary for fertility, and with ZYX-1, a predicted cytoskeletal protein. *Dev. Biol.* **251**, 333-347. doi:10.1006/dbio.2002.0832

Sönnichsen, B., Koski, L. B., Walsh, A., Marschall, P., Neumann, B., Brehm, M., Alleaume, A.-M., Artelt, J., Bettencourt, P., Cassin, E. et al. (2005). Full-genome RNAi profiling of early embryogenesis in Caenorhabditis elegans. *Nature* **434**, 462-469. doi:10.1038/nature03353

Spaulding, E. L., Feidler, A. M., Cook, L. A. and Updike, D. L. (2022). RG/RGG repeats in the C. elegans homologs of Nucleolin and GAR1 contribute to sub-nucleolar phase separation. *Nat. Commun.* **13**, 6585. doi:10.1038/s41467-022-34225-5

Spike, C., Meyer, N., Racen, E., Orsborn, A., Kirchner, J., Kuznicki, K., Yee, C., Bennett, K. and Strome, S. (2008). Genetic analysis of the Caenorhabditis elegans GLH family of P-granule proteins. *Genetics* **178**, 1973-1987. doi:10.1534/genetics.107.083469

Stewart, M. J. and Nordquist, E. K. (2005). Drosophila Bys is nuclear and shows dynamic tissue-specific expression during development. *Dev. Genes Evol.* **215**, 97-102. doi:10.1007/s00427-004-0447-8

Sugihara, K., Sugiyama, D., Byrne, J., Wolf, D. P., Lowitz, K. P., Kobayashi, Y., Kabir-Salmani, M., Nadano, D., Aoki, D., Nozawa, S. et al. (2007). Trophoblast cell activation by trophinin ligation is implicated in human embryo implantation. *Proc. Natl. Acad. Sci. USA* **104**, 3799-3804. doi:10.1073/pnas.0611516104

Sugihara, K., Kabir-Salmani, M., Byrne, J., Wolf, D. P., Lessey, B., Iwashita, M., Aoki, D., Nakayama, J. and Fukuda, M. N. (2008). Induction of trophinin in human endometrial surface epithelia by CGbeta and IL-1beta. *FEBS Lett.* **582**, 197-202. doi:10.1016/j.febslet.2007.12.001

Sun, Y., Yang, P., Zhang, Y., Bao, X., Li, J., Hou, W., Yao, X., Han, J. and Zhang, H. (2011). A genome-wide RNAi screen identifies genes regulating the formation of P bodies in C. elegans and their functions in NMD and RNAi. *Protein Cell* **2**, 918-939. doi:10.1007/s13238-011-1119-x

Suzuki, N., Zara, J., Sato, T., Ong, E., Bakhiet, N., Oshima, R. G., Watson, K. L. and Fukuda, M. N. (1998). A cytoplasmic protein, bystin, interacts with trophinin, tastin, and cytokeratin and may be involved in trophinin-mediated cell adhesion between trophoblast and endometrial epithelial cells. *Proc. Natl. Acad. Sci. USA* **95**, 5027-5032. doi:10.1073/pnas.95.9.5027

Trachtulec, Z. and Forejt, J. (2001). Synteny of orthologous genes conserved in mammals, snake, fly, nematode, and fission yeast. *Mamm. Genome* **12**, 227-231. doi:10.1007/s003350010259

Updike, D. L. and Strome, S. (2009). A genomewide RNAi screen for genes that affect the stability, distribution and function of P granules in Caenorhabditis elegans. *Genetics* **183**, 1397-1419. doi:10.1534/genetics.109.110171

Updike, D. L., Hachey, S. J., Kreher, J. and Strome, S. (2011). P granules extend the nuclear pore complex environment in the C. elegans germ line. *J. Cell Biol.* **192**, 939-948. doi:10.1083/jcb.201010104

Vojtek, A. B. and Hollenberg, S. M. (1995). Ras-Raf interaction: two-hybrid analysis. *Methods Enzymol.* **255**, 331-342. doi:10.1016/S0076-6879(95)55036-4

Voronina, E. and Seydoux, G. (2010). The C. elegans homolog of nucleoporin Nup98 is required for the integrity and function of germline P granules. *Development* **137**, 1441-1450. doi:10.1242/dev.047654

Wang, H., Xiao, W., Zhou, Q., Chen, Y., Yang, S., Sheng, J., Yin, Y., Fan, J. and Zhou, J. (2009). Bystin-like protein is upregulated in hepatocellular carcinoma and required for nucleologenesis in cancer cell proliferation. *Cell Res.* **19**, 1150-1164. doi:10.1038/cr.2009.99

Wojcik, J., Boneca, I. G. and Legrain, P. (2002). Prediction, assessment and validation of protein interaction maps in bacteria. *J. Mol. Biol.* **323**, 763-770. doi:10.1016/S0022-2836(02)01009-4

Xiol, J., Spinelli, P., Laussmann, M. A., Homolka, D., Yang, Z., Cora, E., Couté, Y., Conn, S., Kadlec, J., Sachidanandam, R. et al. (2014). RNA clamping by Vasa assembles a piRNA amplifier complex on transposon transcripts. *Cell* **157**, 1698-1711. doi:10.1016/j.cell.2014.05.018

Yamada, J., Phillips, J. L., Patel, S., Goldfien, G., Calestagne-Morelli, A., Huang, H., Reza, R., Acheson, J., Krishnan, V. V., Newsam, S. et al. (2010). A bimodal distribution of two distinct categories of intrinsically disordered structures with separate functions in FG nucleoporins. *Mol. Cell. Proteomics* **9**, 2205-2224. doi:10.1074/mcp.M000035-MCP201

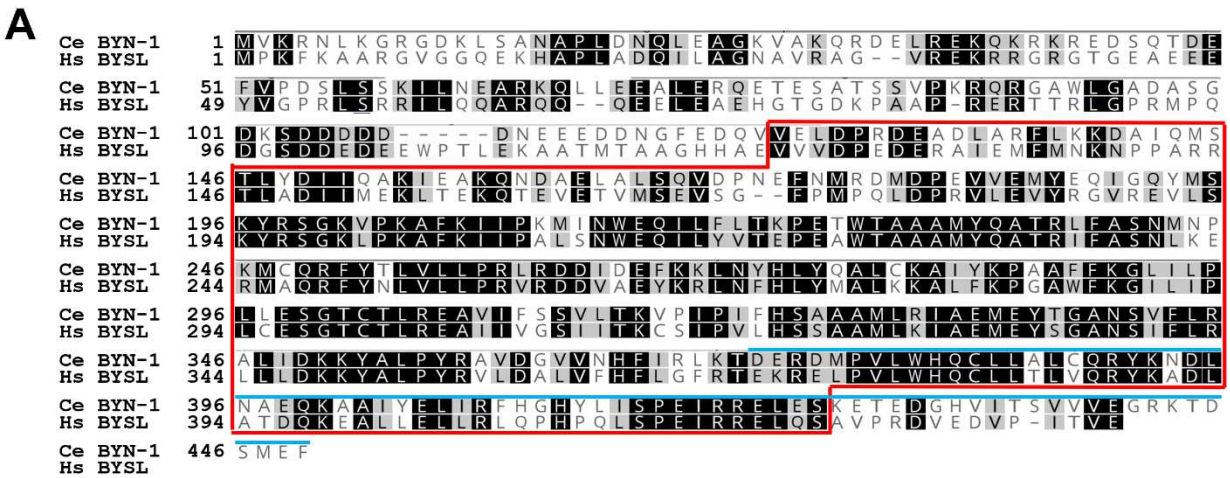

C

Gene name	Percentage ID	Description
glh-2	36.61	C. elegans DEAD-box helicase in P granules
glh-1	36.25	C. elegans DEAD-box helicase in P granules
K01A6.4	33.79	Uncharacterized
ego-2	33.33	C. elegans bro1-domain protein involved in germline proliferation
rde-12	31.58	C. elegans DEAD-box helicase in P granules
glh-4	31.17	C. elegans DEAD-box helicase in P granules
pqn-75	29.19	C. elegans prion-like Q/N-rich protein involved in stress resistance and thermotolerance
NUP98	28.72	Human nuclear pore complex protein
npp-11	27.94	C. elegans nuclear pore complex protein
npp-4	26.86	C. elegans nuclear pore complex protein
npp-10	25.67	C. elegans nuclear pore complex protein
npp-1	24.36	C. elegans nuclear pore complex protein
nlp-14	23.74	C. elegans NLP family neuropeptide
ddx-19	22.82	C. elegans DEAD-box helicase in P granules
npp-7	21.03	C. elegans nuclear pore complex protein
npp-14	18.12	C. elegans nuclear pore complex protein

Fig. S1. Sequence alignment of human Bystin/*C. elegans* BYN-1 and human Trophinin/*C. elegans* FG-rich domains. (A) Conservation of amino acids sequences between Human Byst and *C. elegans* BYN-1. The identity of the protein sequences of human Bystin and *C. elegans* BYN-1 showed 49.55% through Jalview's paired alignment analysis (6). (red box = coiled-coil domain, blue line = GLH-1 interacting domain of BYN-1 as identified by Y2H) (B) *C. elegans* GLH-1 FG repeats aligned to a region of FG repeats in human Trophinin. (C) Percentage of identical protein sequences between human Trophinin and *C. elegans* FG-rich domains. *glh-1* and *glh-2* are the top two proteins that have highest sequence similarity by Jalview's paired alignment analysis. Human NUP98 FG-alignment (grey) with human Trophinin is shown ranked for comparison.

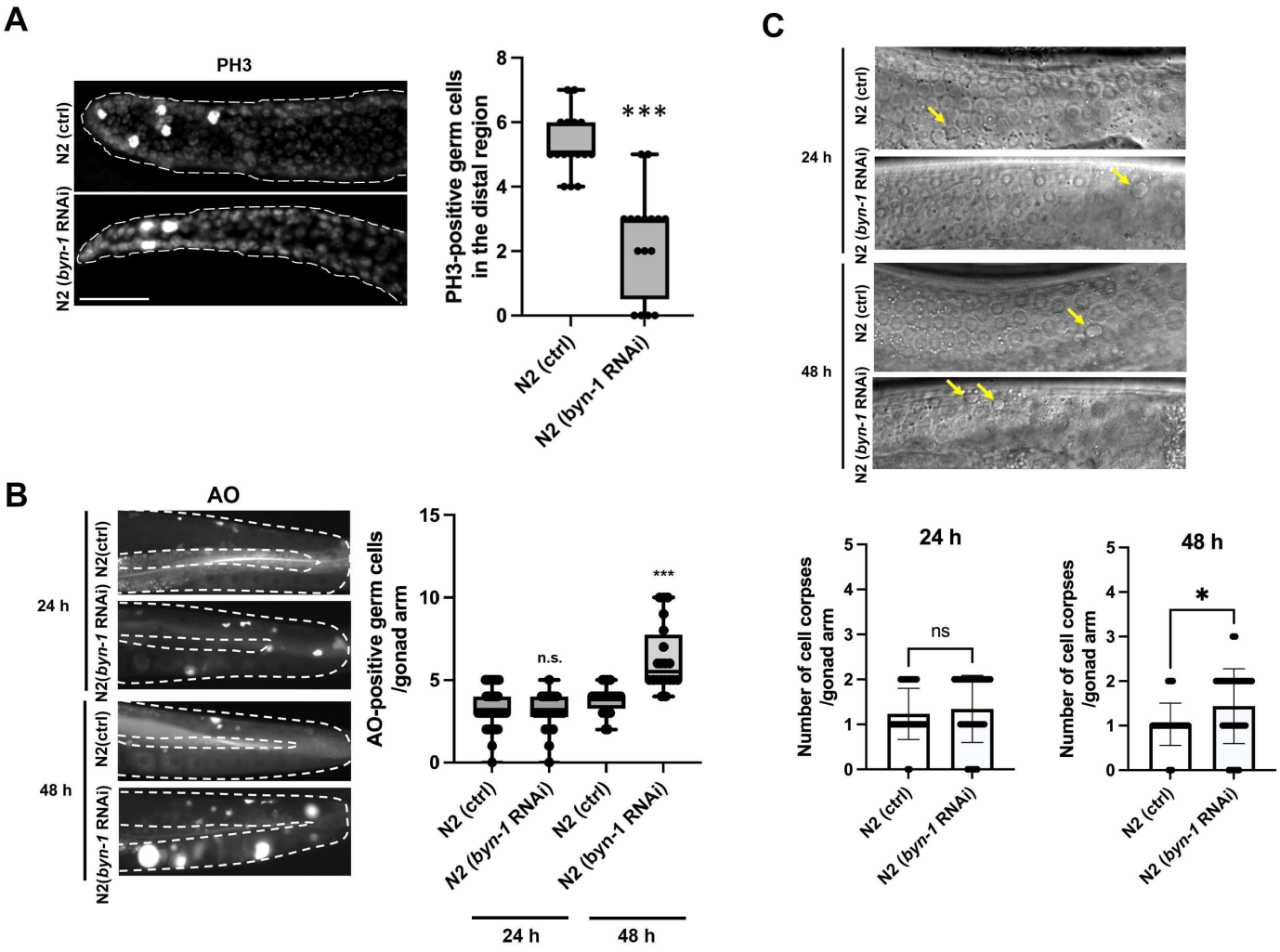

Fig. S2. Depletion of *byn-1* affects germ cell proliferation and apoptosis in *C. elegans*. (A) Left panel: Representative images of PH3-positive germ cells in distal gonadal ends. Dashed lines indicate the shape of gonad arms. Bar, 20 µm. Right panel: Quantification of PH3-positive germ cells in distal gonadal ends per gonad arm (n = 16 in respective conditions). (B) Left panel: Representative images of AO-positive germ cells in the gonad bend at 24 h and 48 h post L4 stage. Right panel: Quantification of AO-positive germ cells per gonad arm (proximal and distal, n ≥ 22 in respective conditions) at 24 h and 48 h post L4 stage. Worms were treated with *byn-1* RNAi at L4 stage at 20 °C. Error bars represent the SD. Statistical significance was calculated using Student's t-test for (A) or One-way ANOVA for (B). ***, $p < 0.001$. n.s., $p > 0.05$. (C) Upper panel: Representative images of germ cell corpses in the gonad at 24 h and 48 h post L4 stage. Lower panel: Average numbers of germ cell corpses per gonad arm (n = 30 ≥ in respective conditions) at 24 h and 48 h post L4 stage in N2. Worms were treated with *byn-1* RNAi at L4 stage at 20 °C. Error bars represent the SD. Statistical significance was calculated using Student's t-test. *, $p < 0.05$. n.s., $p > 0.05$. n.s., p > 0.05.

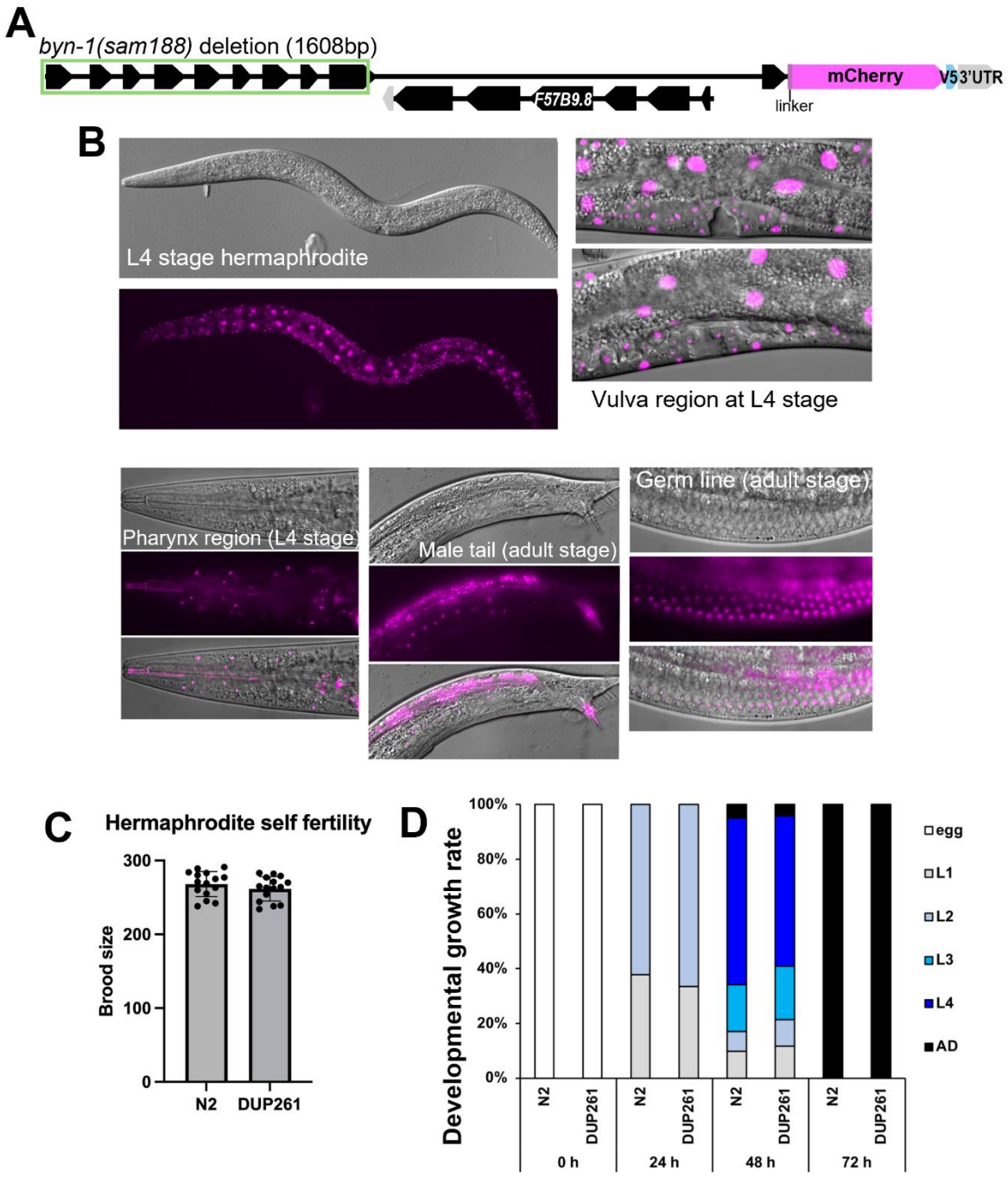

Fig. S3. BYN-1::mCherry::V5 expression and health. (A) Schematic of the mCherry::V5 tag placed on endogenous *byn-1* to generate the DUP261 *glh-1(sam24[glh-1::gfp::3xFlag])* I; *byn-1[sam159(byn-1::mCherry::V5)]* III strain. The *byn-1(sam188)* precision deletion (green box) was created in the DUP261 background, turning off mCherry expression while preserving F57B9.8 encoded within the last intron of *byn-1*. (B) Representative live images of mCherry expression in the germline and soma. (C) The brood size of DUP261 is comparable to wild-type at 20°C, with no noticeable differences in growth rate (D), suggesting the mCherry::V5 tag on *byn-1* presents no deleterious effects.

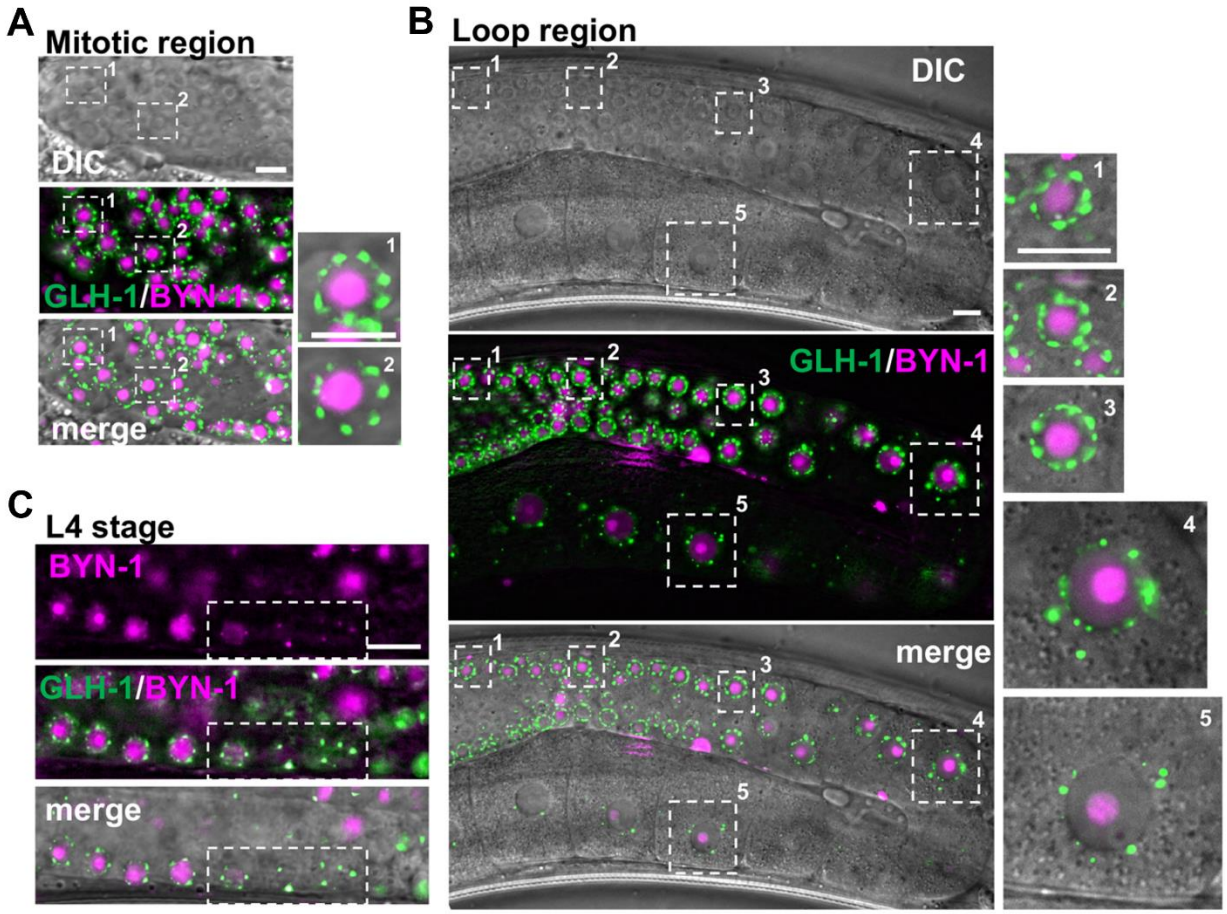

Fig. S4. Localization of GLH-1 and BYN-1 during germline development in *C. elegans*. (A and B) Representative live images showing nucleolar localization of BYN-1 during oogenesis in an adult hermaphrodite. GLH-1 and BYN-1 is visualized in the DUP261 *glh-1(sam24[glh-1::gfp::3xFlag])* I; *byn-1[sam159(byn-1::mCherry::V5)]* III strain at 20 °C. (C) During spermatogenesis in L4 hermaphrodites, BYN-1 is redistributed from the nucleolus to the nucleoplasm, and then from the nucleoplasm into cytoplasmic GLH-1-positive germ granules. Bars, 5 µm.

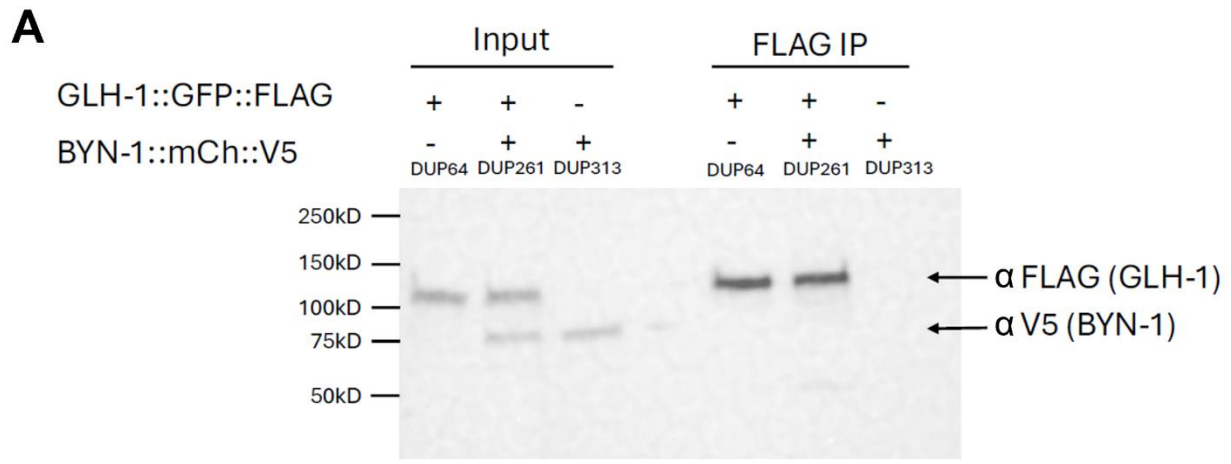

Fig. S5. GLH-1 and BYN-1 fail to coimmunoprecipitate from adult hermaphrodite lysates. (A) Western blot showing expression of endogenous GLH-1 tagged with GFP::3xFLAG and endogenous BYN-1 tagged with mCherry::V5 in three strains, DUP64 *glh-1(sam24[glh-1::gfp::3xFlag])* I, DUP261 *glh-1(sam24[glh-1::gfp::3xFlag])* I; *byn-1[sam159(byn-1::mCherry::V5)]* III, and DUP313 *byn-1[sam159(byn-1::mCherry::V5)]* III. The BYN-1::mCh::V5 is not detected in the FLAG IP.

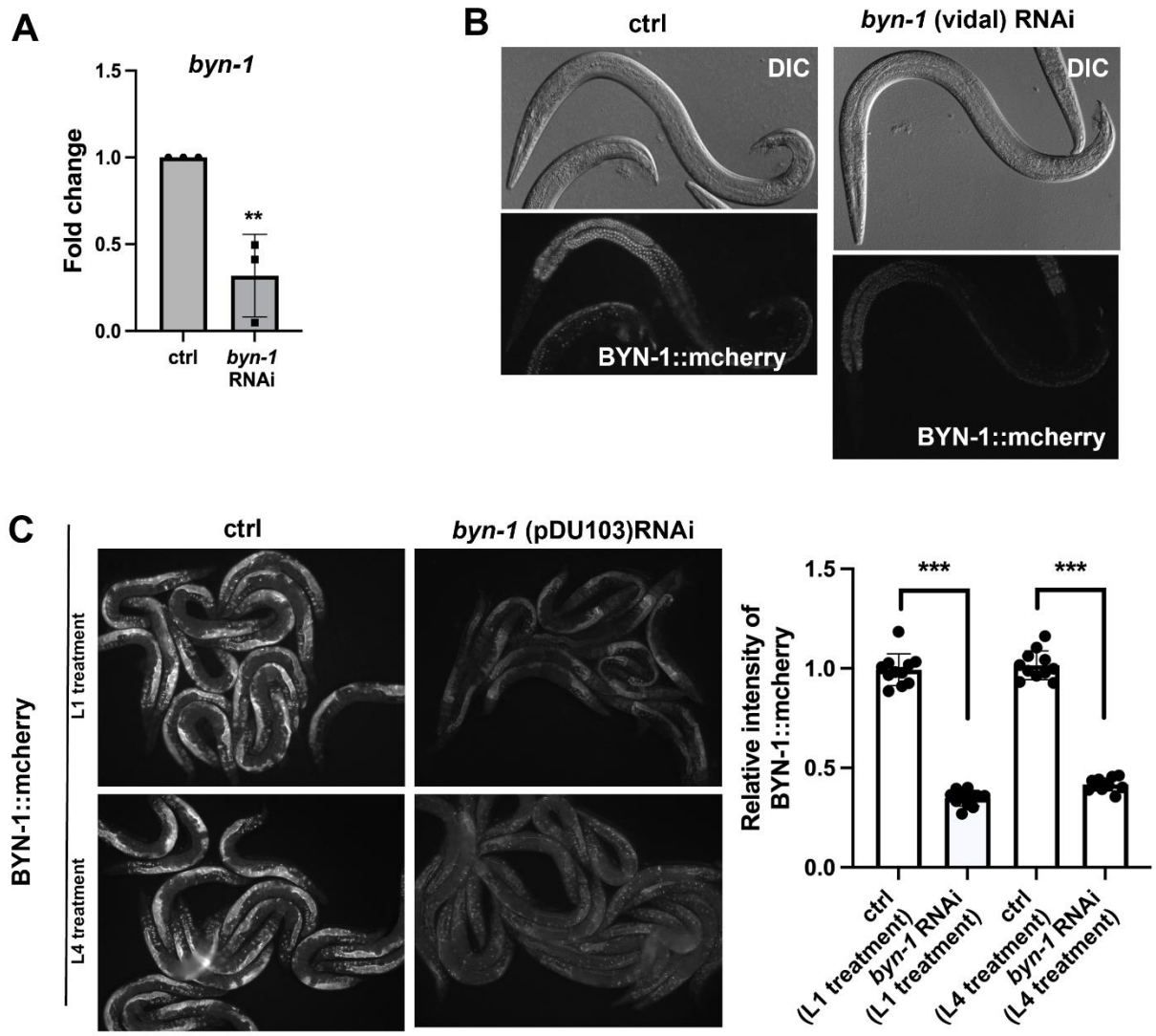

Fig. S6. Depletion of *byn-1* with RNAi feeding. (A) Quantitative RT-PCR of *byn-1* shows depletion in adult progeny of hermaphrodites fed *byn-1* RNAi (Vidal orfeome clone) as L4s. (B) Representative images of BYN-1::mCherry expression in male progeny of *byn-1* RNAi (Vidal) fed worms. (C) BYN-1::mCherry intensity is decreased in progeny of hermaphrodites fed HT115 bacteria harboring an independent *byn-1* RNAi plasmid (pDU103). Graph shows the decrease in BYN-1::mCherry intensity quantified with ImageJ. Student's t-test, ***, $p<0.001$.

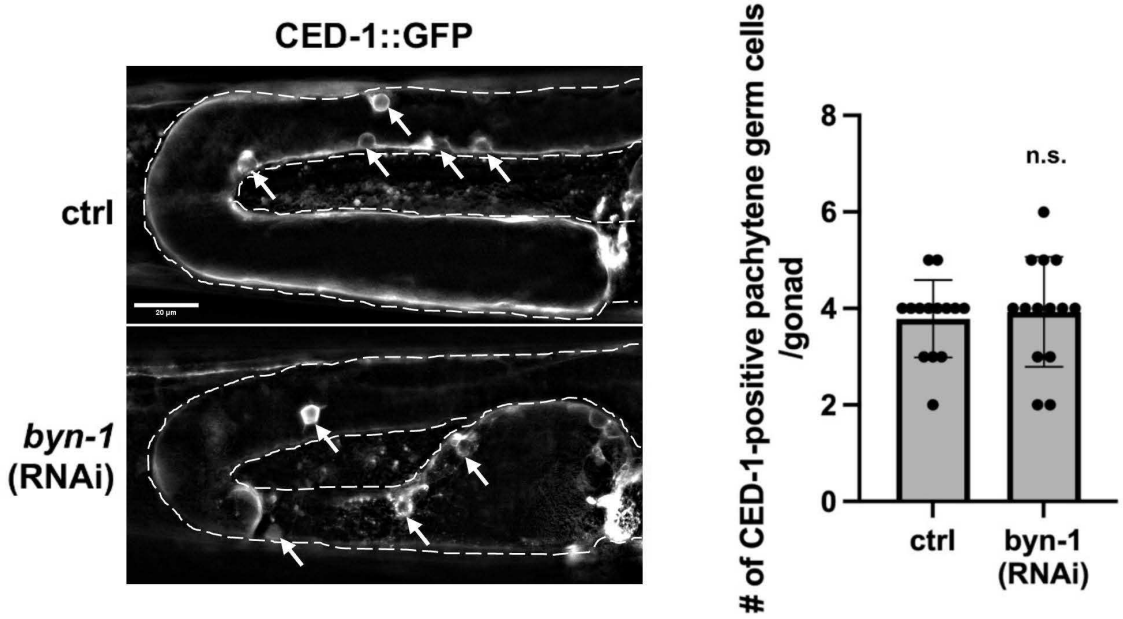

Fig. S7. Depletion of *byn-1* in hermaphrodite shows a normal CED-1::GFP activation at 24 h post L4 stage. Cell corpses engulfment visualized with *smIs34[ced-1p::ced-1::GFP]* transgene at 20 °C. Some of the engulfed germ cell corpses surrounded by the GFP-tagged CED-1 (CED-1::GFP) signal are marked with white arrows. The number of CED-1-positive germ cells by the GFP-tagged CED-1 signal per gonad arm at 24 h post L4 stage in hermaphrodite. Error bars represent the SD. Statistical significance was calculated using Student's t-test. n.s., $p > 0.05$. Bar, 20 μm.

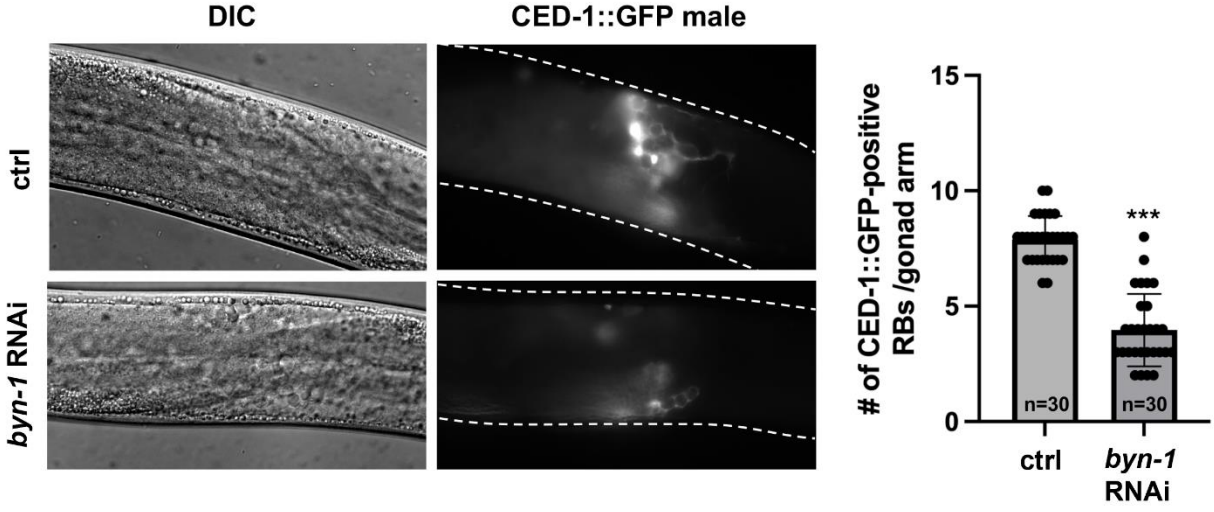

Fig. S8. Depletion of *byn-1* in male shows a decreased CED-1::GFP activation at 24 h post L4 stage. RB engulfment visualized with *smIs34[ced-1p::ced-1::GFP]* transgene at 20 °C. The number of CED-1-positive RBs by the GFP-tagged CED-1 signal per gonad arm at 24 h post L4 stage in males. Error bars represent the SD. Statistical significance was calculated using Student's t-test. n.s., $p > 0.001$.

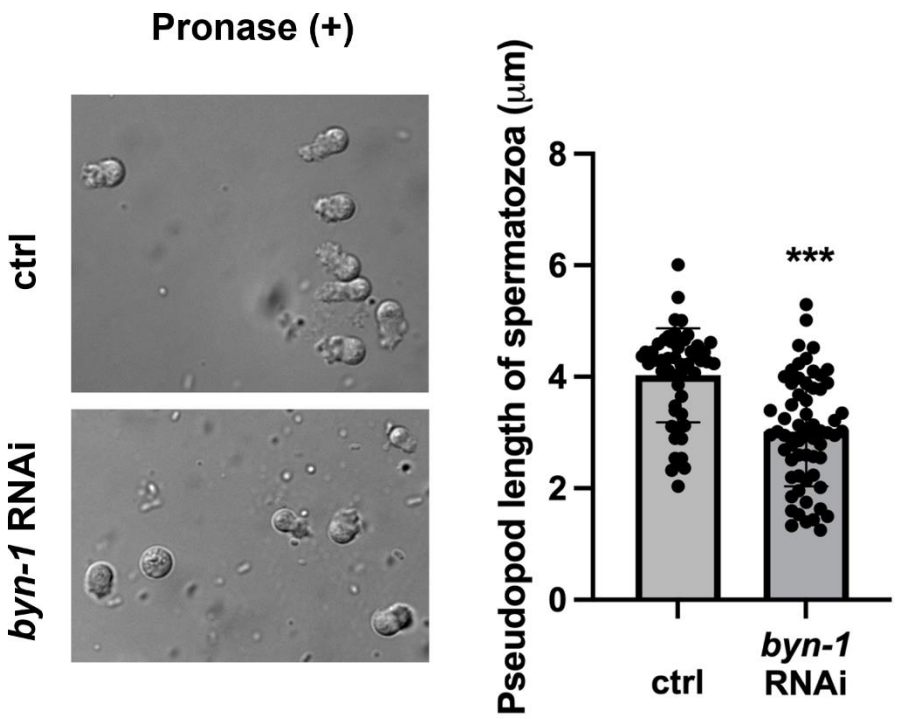

Fig. S9. Quantification of the pseudopod length in spermatozoa. *In vitro* activation of sperm from wild-type (N2) males fed control and *byn-1* RNAi with pronase. The length of the pseudopod was measured as a distance from the root of the pseudopod to its farthest tip. More than 50 spermatozoa of each condition were examined. Error bars indicate s.d. ***$p < 0.001$ (Student's t-test).

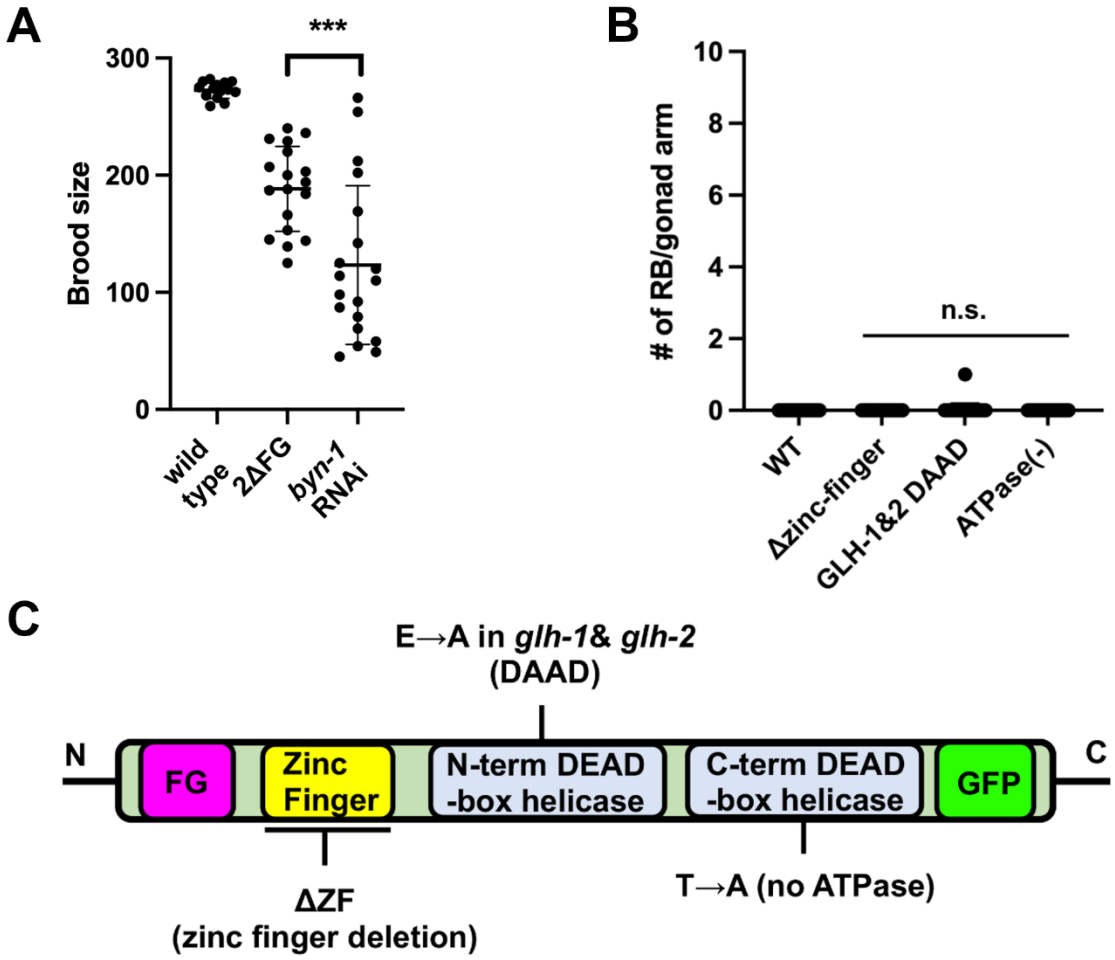

Fig. S10. Brood size and RB accumulation in *glh-1* mutants. (A) Brood size of 2ΔFG compared to wild-type and *byn-1* RNAi animals. Student's t-test, ***p<0.001. (B) RB accumulation is not affected in *glh-1* zinc-finger and helicase mutants. RBs were quantified in hermaphrodites 24 h post L4 stage. n=30 for WT, n=30 for ΔZF mutant, n=34 for DAAD double mutant, n=27 for T to A ATPase mutant. One-way ANOVA n.s. > 0.05. (C) Schematic showing mutation details in GLH-1.

Table S1. Six high confidence interacting proteins of GLH-1 by yeast-two-hybrid screen.

Gene Name	Description	Predicted Biological Score (PBS)	Clones
eif-3.G	Eukaryotic Translation Initiation Factor	A – very high confidence	17
gpd-3	GPD (Glyceraldehyde 3-Phosphate Dehydrogenase)	A – very high confidence	23
gyg-1	GIYcoGenin like, predicted to be involved in glycogen biosynthetic processes	A – very high confidence	46
F55F8.2	Ortholog of human DDX24 (DEAD-box helicase 24)	A – very high confidence	11
byn-1	Mammalian BYstiN related (adhesion protein)	B – high confidence	6
znf-598	ZiNc Finger protein homolog	B – high confidence	14